

LOCAL/GLOBAL ANALYSIS OF THE STATIONARY SOLUTIONS OF SOME NEURAL FIELD EQUATIONS*

ROMAIN VELTZ[†] AND OLIVIER FAUGERAS[‡]

Key words. neural field equations, stationary solutions, bifurcation, Leray-Schauder degree, ring model.

AMS subject classifications. 34C23, 34D20, 34D23, 34G20, 34L15, 37K50, 37M20, 45G15, 45P05, 46E35, 47H11, 47H30, 55M25, 58C40, 92B20, 92C20

Abstract. Neural or cortical fields are continuous assemblies of mesoscopic models, also called neural masses, of neural populations that are fundamental in the modeling of macroscopic parts of the brain. Neural fields are described by nonlinear integro-differential equations. The solutions of these equations represent the state of activity of these populations when submitted to inputs from neighbouring brain areas. Understanding the properties of these solutions is essential in advancing our understanding of the brain. In this paper we study the dependency of the stationary solutions of the neural fields equations with respect to the stiffness of the nonlinearity and the contrast of the external inputs. This is done by using degree theory and bifurcation theory in the context of functional, in particular infinite dimensional, spaces. The joint use of these two theories allows us to make new detailed predictions about the global and local behaviours of the solutions. We also provide a generic finite dimensional approximation of these equations which allows us to study in great details two models. The first model is a neural mass model of a cortical hypercolumn of orientation sensitive neurons, the ring model [49]. The second model is a general neural field model where the spatial connectivity is described by heterogeneous Gaussian-like functions.

1. Introduction. Neural or cortical fields are continuous assemblies of mesoscopic models, also called neural masses, of neural populations that are essential in the modeling of macroscopic parts of the brain.

They were first studied by Wilson and Cowan, Amari [52, 2] and play an important role in the design of the models of the visual cortex such as those proposed by Bressloff [12]. Neural fields describe the mean activity of neural populations by nonlinear integro-differential equations. The solutions of these equations represent the state of activity of these populations either in isolation, one talks about intrinsic activity, or when submitted to inputs from neighbouring brain areas. Understanding the properties of these solutions is therefore important for advancing our understanding of how the brain encodes and processes its internal and external inputs.

Among these solutions, the persistent states (or stationary solutions) are important for at least two reasons. First, in the case of autonomous systems, looking for persistent states helps to understand the dynamics because they are an easy way to divide the phase space into smaller components. If one makes the further assumption that the connectivity function (to be defined below) is symmetric (see the review by [20]), the dynamics is described by heteroclinic orbits connecting the stationary solutions. Second, they are thought to be good models of the memory holding tasks on the time scale of the second, as demonstrated by experimentalists on primates [15, 27, 42].

There are four major ingredients that occur in the mathematical description of these equations. First, the domain Ω of integration (typically a piece of cortex) which is of dimension d and can be bounded or unbounded, second, the type of the nonlinearity (sigmoidal, Heaviside), third, the type of the connectivity function that appears in the integral (homogeneous, i.e. translation invariant, or heterogeneous), and fourth, the number p of neuronal populations that are modeled.

*This work was partially supported by the ERC grant 227747 - NERVI and the EC IP project #015879 - FACETS

[†]IMAGINE/LIGM, Université Paris Est and NeuroMathComp team.

[‡]Corresponding author, NeuroMathComp team, INRIA, CNRS, ENS Paris, olivier.faugeras@sophia.inria.fr

Working with an unbounded domain Ω is not biologically relevant and also raises some mathematical difficulties. Our work is with a bounded Ω . Besides its biological relevance, this hypothesis is **crucial** for our mathematical analysis: it implies that there is at least one persistent state for any set of parameter values and provides bounds for these persistent states. We discuss the numerical validity of this hypothesis in section 7.

The nonlinearity in the neural field equations is most of the time chosen to be a Heaviside function which leads to several mathematical difficulties, one of them being the specification of the correct functional space. We found easier in [26] to use smooth nonlinear functions instead, to study the persistent states. Only a few papers use sigmoidal functions, e.g., [3, 51], or an alpha function¹, [40]. Moreover, Pinto and Ermentrout have shown how to extend results obtained with Heaviside functions to results holding for smooth sigmoids using singular perturbation theory [44], while in [37, 22] fixed points theorems are used to prove results for sigmoids. Let us also mention the fact that some perturbative results for smooth sigmoids have been obtained in the case of weakly interacting pulses [9] and inhomogeneous traveling waves [6, 36]. In this paper we make the assumption that the nonlinearity is a sigmoid function, i.e. infinitely differentiable.

Regarding the connectivity function we only assume that it is square integrable, as well as some of its derivatives, see section 2.1. Hence it can be heterogeneous, i.e. not translation invariant as it is often assumed in the literature. Despite the fact that they are rarely considered, networks with heterogeneous weights have been studied in previous publications [34, 45, 6, 7, 36, 47]. Our work provides a firmer mathematical setting to and generalizes these attempts.

Surprisingly, there are few papers dealing with the persistent states. Their authors use two main methods: Turing patterns (or bifurcation theory) and reduction to ODEs and PDEs.

The first method is used in almost every paper, e.g. [3, 17, 5, 51], very often in the case of a translation invariant connectivity function (hence a convolution kernel), and leads to the description of a large amount of solutions and behaviours thereof such as traveling waves, breathers, persistent states, etc. . . that depend on special relations between the spatial frequency k and the temporal frequency, ω . We generalize this approach as follows: we do not worry about the spatial structure of the cortical states (i.e. the solutions, indexed by the spatial frequency k in these previous studies) but think instead of a cortical state as a point in a (functional) vector space. We can then elegantly and economically study how this point trajectory varies (bifurcates) when the relevant parameters in the neural field equations vary. By doing so we are able to harvest a lot more results that do not depend upon the translation invariant assumption but of course also hold in this case.

The second method is to reduce the search for the persistent states to the problem of finding homoclinic orbits for some ODEs [39] when $\Omega = \mathbb{R}$ and $p = 1$, or of finding of homoclinic orbits for some PDEs [40] ff $\Omega = \mathbb{R}^2$. The obvious advantage of these approaches is that one can use finite-dimensional tools such as those described in [38, 28], or PDE methods, such as those described for example in [32], for the bifurcation analysis. When successful, these approaches allow to compute the persistent states independently of their stability and to compute their number as a function of the strength of the connections.

In a previous paper [26], we started the analysis of the neural fields equations defined over a finite part of the cortex from two different viewpoints, theoretical and numerical. We proved some results concerning the dynamics and gave a method to efficiently compute the persistent state (or stationary solution) under the assumption that it was unique.

In the same article, we unsurprisingly found that the dynamics was “boring” (every initial

¹ $e^{-1/v^2} H(v)$, H the Heaviside function.

condition converged to a single persistent state) if the stiffness of the nonlinearity was small. For example the system could not exhibit oscillatory behaviours. More importantly we did not produce a method for computing more than one, or even all the persistent states when the system featured several such states.

In this paper we relax the hypothesis leading to the uniqueness of the persistent state and try to understand the structure of the set, noted \mathcal{B} , of stationary solutions as the parameters² vary over large ranges of values, thereby departing from a purely local analysis. The local structure of the set \mathcal{B} is described using bifurcation theory (see [41, 32, 30]) whereas degree theory helps to understand its global structure. This latter theory can predict the existence of stationary solutions that cannot be obtained using only bifurcation theory. In order to compute numerically these persistent states, we use a multiparameter continuation scheme that allows to compute non-connected branches³ of persistent states that would otherwise be unattainable.

In order to perform our numerical experiments we consider a very general method for approximating the connectivity kernels, the Pincherle-Goursat kernels method [50], which allows to reduce exactly the dynamics to a system of ODEs whose dimension is directly related to the level of approximation and can be arbitrarily large, if needed. Hence our choice to use infinite dimensional techniques to the integral equation is guided by the fact that it offers a simple, albeit abstract, conceptual framework in which the behaviours of interest to us can be described in a clean and dimension-independent manner. When it comes to numerical experiments we use the system of ODEs provided by the Pincherle-Goursat kernels.

The paper is organized as follows. In section 2 we introduce the functional analysis framework that allows us to study the neural field equations as a Cauchy problem in a functional space and to derive a number of useful properties of the (stationary) solutions of these equations. In section 3 we combine the results of the previous section with a bifurcation study in order to obtain more information about the set \mathcal{B} of solutions. A numerical scheme is proposed to compute the structure of this set. In section 4 we show how to reduce the neural field equations to a set of ODEs with an arbitrary precision through the use of the Pincherle-Goursat kernels. In section 5 we study in detail a neural mass model that reduces exactly to a finite set of ODEs, the ring model. In section 6, we compute the stationary solutions for a model featuring two populations of neurons on a two-dimensional cortex sheet connected by heterogenous Gaussian-like functions: it allows us to provide salient examples of the predictions obtained in sections 2 and 3. In section 7 we discuss the biological and numerical validity of two of our main hypotheses, the fact that the cortex has a finite size and the use of a smooth sigmoid instead of a Heaviside function. We conclude in section 8.

2. General framework. We consider the following formal neural field equation defined over a bounded piece of cortex and/or feature space $\Omega \subset \mathbb{R}^d$. We wish to encompass in the same formalism the geometry of the cortex, seen as a bounded piece of \mathbb{R}^d , $d = 1, 2, 3$, and the geometry of such feature spaces as edge or motion orientations (directions) which are represented by a value between 0 and π (2π), or scale which is represented by a positive number, e.g. the spatial frequency. In section 5 we analyze in detail an example where the focus is on edge directions while in section 6 we analyze another example in which the focus is on the two-dimensional geometry of the cortex.

$$\begin{cases} \dot{\mathbf{V}}(\mathbf{r}, t) &= -\mathbf{L} \cdot \mathbf{V}(\mathbf{r}, t) + [\mathbf{J}(t) \cdot \mathbf{S}(\lambda(\mathbf{V}(t) - \boldsymbol{\theta}))](\mathbf{r}) + \mathbf{I}_{ext}(\mathbf{r}, t) & t > 0 \\ \mathbf{V}(\cdot, 0) &= \mathbf{V}_0(\cdot) \end{cases} \quad (2.1)$$

²We use the stiffness of the nonlinearity and the contrast of the external inputs but our analysis applies to other parameters.

³A branch is a one-dimensional set of stationary solutions obtained by varying one parameter.

This equation is an initial value problem that describes the time variation of the p -dimensional vector function \mathbf{V} defined on Ω , starting from the initial condition \mathbf{V}_0 , a function defined on Ω . At each time $t \geq 0$ \mathbf{V} belongs to some functional space, in effect a Hilbert space \mathcal{F} , that we describe in the next section. We now discuss the various quantities that appear in (2.1).

$\mathbf{J}(t)$ is a linear operator from \mathcal{F} to itself defined by:

$$[\mathbf{J}(t) \cdot \mathbf{V}(t)](\mathbf{r}) = \int_{\Omega} \mathbf{J}(\mathbf{r}, \mathbf{r}', t) \mathbf{V}(\mathbf{r}', t) d\mathbf{r}', \quad (2.2)$$

where $\mathbf{J}(\mathbf{r}, \mathbf{r}', t)$ is a $p \times p$ matrix that describes the ‘‘strength’’ of the connections. We also describe in the next section the functional space to which $\mathbf{J}(t)$ belongs and the conditions it must satisfy in order for the equation (2.1) to be well-defined.

The external current input, $\mathbf{I}_{ext}(\cdot, t)$, is in \mathcal{F} for all $t \geq 0$.

The function $\mathbf{S} : \mathbb{R}^p \rightarrow \mathbb{R}^p$ is defined by $\mathbf{S}(x) = [S(x_1), \dots, S(x_p)]^T$, where $S : \mathbb{R} \rightarrow (0, 1)$ is the normalized sigmoid function of equation

$$S(z) = \frac{1}{1 + e^{-z}}. \quad (2.3)$$

It is infinitely differentiable on \mathbb{R}^p and all its derivatives $S^{(q)}(x)$, $q = 1, 2, \dots$ are bounded. For all integer $q \geq 1$ we note $\mathbf{S}^{(q)}(x)$ the $p \times p$ diagonal matrix $\text{diag}(S^{(q)}(x_1), \dots, S^{(q)}(x_p))$. Because of the form of the function \mathbf{S} , the q th order derivative of \mathbf{S} at $x \in \mathbb{R}^p$ is the multilinear function defined by

$$D^q \mathbf{S}(x) \cdot (y_1, \dots, y_q) = \mathbf{S}^{(q)}(x) \cdot (y_1 \cdots y_q), \quad y_i \in \mathbb{R}^p, i = 1, \dots, q \quad (2.4)$$

where $y_1 \cdots y_q$ is the component pointwise product of the q vectors y_1, \dots, y_q of \mathbb{R}^p , i.e. the vector of \mathbb{R}^p whose k th coordinate, $k = 1, \dots, p$ is equal to the product of the q k th coordinates of each vector y_i , $i = 1, \dots, q$.

λ is the $p \times p$ diagonal matrix $\text{diag}(\lambda_1, \dots, \lambda_p)$, $\lambda_i \geq 0$, $i = 1, \dots, p$ that determines the slope of each of the p sigmoids at the origin. We note λ_m the maximum value of the λ_i s.

θ is a p -dimensional vector that determines the threshold of each of the p sigmoids, i.e. the value of the membrane potential corresponding to 50% of the maximal activity.

The diagonal $p \times p$ matrix \mathbf{L} is equal to $\text{diag}(\frac{1}{\tau_1}, \dots, \frac{1}{\tau_p})$, where the positive numbers τ_i , $i = 1, \dots, p$ determine the exponential decrease dynamics of each neural population.

As recalled in the introduction and detailed in [24, 25] this equation corresponds to a mesoscopic description of population of neurons which is called voltage-based by Ermentrout [20]. \mathbf{V} in equation (2.1) therefore has the biological interpretation of an average membrane potential of p populations of neurons. As pointed out by the same authors, there is also an activity-based mesoscopic description which leads to the following initial value problem:

$$\begin{cases} \dot{\mathbf{A}}(\mathbf{r}, t) &= -\mathbf{L}_a \cdot \mathbf{A}(\mathbf{r}, t) + \mathbf{S}(\lambda([\mathbf{J}(t) \cdot \mathbf{A}](\mathbf{r}, t) + \mathbf{I}_{ext}(\mathbf{r}, t))) \quad t > 0 \\ \mathbf{A}(\cdot, 0) &= \mathbf{A}_0(\cdot) \end{cases} \quad (2.5)$$

$\mathbf{L}_a \neq \mathbf{L}$ (see [20]) because they do not have the same biological meaning: One is related to the synaptic time constant and the other to the cell membrane time constant. We let $\mathbf{L}_a = \text{diag}(\alpha_1, \dots, \alpha_p)$.

The two problems (2.1) and (2.5) are closely related. In particular there is a one to one correspondence between their equilibria, as recalled below for the ring model of section 5, which is an activity-based model.

2.1. Choice of the appropriate functional space. The problem at hand is to find an appropriate mathematical setting, i.e. to choose the functional space \mathcal{F} , for the neural field equations based on three criteria 1) problems (2.1) and (2.5) should be well-posed, 2) its biological relevance and 3) its ability to allow numerical computations.

A Hilbert space is appealing because of its metric structure induced by its inner product. Hence, a natural choice arising from the definition of the linear operator \mathbf{J} would be the space $\mathbf{L}^2(\Omega, \mathbb{R}^p)$. But this space allows the average membrane potential to be singular which is biologically excluded. For example the function $\mathbf{r} \rightarrow |\mathbf{r}|^{-1/2} \in \mathbf{L}^2(\Omega, \mathbb{R}^p)$ if $d \geq 0$. It would be desirable that this potential be bounded on the cortex. A way to achieve this is to allow for more spatial regularity of the membrane potential: it is **reasonable**, E.g., from optical imaging measurements. to choose $\mathbf{r} \rightarrow \mathbf{V}(\mathbf{r})$ as being differentiable almost everywhere.

For technical reasons that will become clear later we choose the Sobolev space

$$\mathcal{F} = \mathbf{W}^{m,2}(\Omega, \mathbb{R}^p), \quad m \in \mathbb{N},$$

with the inner product:

$$\langle \mathbf{X}_1, \mathbf{X}_2 \rangle_{\mathcal{F}} = \sum_{|\alpha|=0}^m \langle D^\alpha \mathbf{X}_1, D^\alpha \mathbf{X}_2 \rangle_{\mathbf{L}^2(\Omega, \mathbb{R}^p)}, \quad \forall \mathbf{X}_1, \mathbf{X}_2 \in \mathcal{F}, \quad (2.6)$$

where, as usual, the multi-index α is a sequence $\alpha = (\alpha_1, \dots, \alpha_d)$ of positive integers, $|\alpha| = \sum_{i=1}^d \alpha_i$, and the symbol D^α represents a partial derivative:

$$D^\alpha \varphi = \frac{\partial^{\alpha_1 + \dots + \alpha_d} \varphi}{\partial r_1^{\alpha_1} \dots \partial r_d^{\alpha_d}},$$

where $\varphi : \Omega \rightarrow \mathbb{R}$ and $\mathbf{r} = (r_1, \dots, r_d)$.

Note that $\mathcal{F} = \underbrace{W^{m,2}(\Omega) \times \dots \times W^{m,2}(\Omega)}_p$. Later we use the notation \mathcal{G} for $W^{m,2}(\Omega)$,

i.e. $\mathcal{F} = \mathcal{G}^p$.

2.1.1. Choosing the value of m . The value of the integer m determines the regularity of the functions \mathbf{V} that represent the cortical states as well as that of the connectivity function \mathbf{J} . It turns out that, depending upon the relative values of m and the dimension $d = 1, 2, 3$ of the space where we represent the cortical patch Ω and/or the feature space, \mathcal{F} is a (commutative) Banach algebra for the pointwise multiplication. This is important when using bifurcation theory because we need to use Taylor expansions of the right-hand-side of (2.1).

Being a Banach algebra property requires some regularity of Ω , i.e. of its boundary $\partial\Omega$. Because in the numerical experiments of section 6 we work with the open square $\Omega = [-1, 1]^2$, we will assume the weakest regularity, the so-called cone property, see [1, Chapter IV] for a definition. In practice one can safely assume that $\partial\Omega$ is C^1 . Roughly speaking it means that this boundary is a C^1 -manifold of dimension $d - 1$ of \mathbb{R}^d . The exact definition, called the uniform C^1 -regularity, can again be found in [1, Chapter IV]. It implies some weaker regularity assumptions, such as the cone property.

Under this assumption on Ω we can adapt the theorem in [1, Chapter V, Theorem 5.24] to obtain the following result :

COROLLARY 2.1. *If the relation $2m > d$ holds, then \mathcal{F} is a commutative Banach algebra with respect to component pointwise multiplication, i.e. for all \mathbf{U} and \mathbf{V} elements of \mathcal{F} their component pointwise product \mathbf{UV} is in \mathcal{F} and there exists a positive constant K^* such that*

$$\|\mathbf{UV}\|_{\mathcal{F}} \leq K^* \|\mathbf{U}\|_{\mathcal{F}} \|\mathbf{V}\|_{\mathcal{F}} \quad \forall \mathbf{U}, \mathbf{V} \in \mathcal{F},$$

where $\mathbf{UV} = (\mathbf{U}_1 \mathbf{V}_1, \dots, \mathbf{U}_p \mathbf{V}_p)$.

Let us explore some consequences of this proposition on our possible choices for the value of m . These choices are guided by the idea of constraining the functional space \mathcal{F} as little as possible, given the fact that $\mathbf{W}^{m,2} \subset \mathbf{W}^{n,2}$ for all integers $0 \leq n < m$

$d = 1$: The relation $2m > 1$ implies $m \geq 1$ and we choose $m = 1$.

$d = 2, 3$: The relation $2m > d$ implies $m \geq 2$ and we choose $m = 2$.

Similar results hold for higher values of the dimension d but these cover the cases discussed in this article.

We summarize all this in the following proposition

PROPOSITION 2.2 (Choice of \mathcal{F}). *If Ω is has the cone property, in particular if it is uniformly C^1 -regular, then we have $\mathcal{F} = \mathbf{W}^{1,2}(\Omega, \mathbb{R}^p)$ for $d = 1$ and $\mathcal{F} = \mathbf{W}^{2,2}(\Omega, \mathbb{R}^p)$ for $d = 2, 3$. In all three cases, \mathcal{F} is a commutative Banach algebra with respect to component pointwise multiplication.*

2.1.2. The choice of \mathbf{J} . We assume that $\mathbf{J}(\cdot, \cdot, t) \in \mathbf{W}^{m,2}(\Omega \times \Omega, \mathbb{R}^{p \times p})$ for all $t > 0$.

As a consequence, the Frobenius \mathcal{F} -norm of the linear operator $\mathbf{W}(t)$, noted $\|\mathbf{J}(t)\|_{\mathcal{F}}$, is well-defined

$$\|\mathbf{J}(t)\|_{\mathcal{F}}^2 = \sum_{|\alpha|, |\alpha'|=0}^m \int_{\Omega \times \Omega} \left\| D^\alpha D^{\alpha'} \mathbf{J}(\mathbf{r}, \mathbf{r}', t) \right\|_F^2 d\mathbf{r} d\mathbf{r}',$$

where it is understood that the partial derivative operator D^α (respectively $D^{\alpha'}$) acts on the variable \mathbf{r} (respectively \mathbf{r}') and $\|\mathbf{J}(\mathbf{r}, \mathbf{r}', t)\|_F$ is the Frobenius norm of the matrix $\mathbf{J}(\mathbf{r}, \mathbf{r}', t)$,

$$\|\mathbf{J}(\mathbf{r}, \mathbf{r}', t)\|_F^2 = \sum_{i,j} J_{ij}(\mathbf{r}, \mathbf{r}', t)^2$$

This hypothesis also ensures the existence of the operator \mathbf{J} as a linear operator from \mathcal{F} to \mathcal{F} .

PROPOSITION 2.3. *Assume that $\mathbf{J}(\cdot, \cdot, t) \in \mathbf{W}^{m,2}(\Omega \times \Omega, \mathbb{R}^{p \times p})$ for all $t > 0$. Then equation (2.2) defines a linear operator from \mathcal{F} to \mathcal{F} .*

Proof. see appendix A \square

Since \mathbf{S} is a \mathbb{R}^p -valued bounded function on Ω and such functions are in $\mathbf{L}^2(\Omega)$ the right-hand side of (2.1) is an element of \mathcal{F} . Similarly, because \mathbf{S} is also infinitely differentiable and all its derivatives bounded, the right-hand side of (2.5) is an element of \mathcal{F} .

Finally we note $\|\mathbf{J}(t)\|$ the operator norm of $\mathbf{J}(t)$, i.e.

$$\sup_{\|\mathbf{V}\|_{\mathcal{F}} \leq 1} \frac{\|\mathbf{J}(t) \cdot \mathbf{V}\|_{\mathcal{F}}}{\|\mathbf{V}\|_{\mathcal{F}}}$$

It is known, see e.g. [35], that

$$\|\mathbf{J}(t)\| \leq \|\mathbf{J}(t)\|_{\mathcal{F}}$$

Remark 1. Note that the relation $2m > d$ and our regularity assumption on Ω , imply, through the so-called Sobolev imbedding theorem, [1, Chapter V, lemma 5.15], that

$$\mathcal{G} \rightarrow C_B^0(\Omega),$$

where $C_B^0(\Omega)$ is the set of continuous bounded functions on Ω . The consequence is that the state vectors \mathbf{V} and the connectivity matrix \mathbf{J} are essentially bounded, which has certainly the right biological flavor.

2.2. The Cauchy problem. In this section we prove that equation (2.1) is well-posed and provide some properties of its solutions.

We rewrite it as a Cauchy Problem, i.e. as an ordinary differential equation on the functional space \mathcal{F} . This turns out to be convenient for the upcoming computations.

$$\begin{cases} \frac{d\mathbf{V}}{dt} &= -\mathbf{L} \cdot \mathbf{V} + \mathbf{R}(t, \mathbf{V}) & t > 0 \\ \mathbf{V}(0) &= \mathbf{V}_0 \in \mathcal{F} \end{cases} \quad (2.7)$$

The nonlinear operator \mathbf{R} is defined by

$$\mathbf{R}(t, \mathbf{V}) = \mathbf{J}(t) \cdot \mathbf{S}(\boldsymbol{\lambda}(\mathbf{V} - \boldsymbol{\theta})) + \mathbf{I}_{\text{ext}}(t) \quad (2.8)$$

Proposition 2.3 shows that $\mathbf{R}(t, \cdot) : \mathcal{F} \rightarrow \mathcal{F}$ for all $t > 0$. We have the further properties:

LEMMA 2.4. \mathbf{R} satisfies the following properties :

- \forall integer $q \geq 0$, $\mathbf{R}(t, \cdot) \in C^q(\mathcal{F}, \mathcal{F})$ and $D^q \mathbf{R}(t, \mathbf{V}_0) = \boldsymbol{\lambda}^q \mathbf{J}(t) \mathbf{S}^{(q)}(\boldsymbol{\lambda}(\mathbf{V}_0 - \boldsymbol{\theta}))$ for all \mathbf{V}_0 in \mathcal{F} .
- $\|\mathbf{R}(t, \mathbf{U}_1) - \mathbf{R}(t, \mathbf{U}_2)\|_{\mathcal{F}} \leq \lambda_m \|\mathbf{J}(t)\|_{\mathcal{F}} \|\mathbf{U}_1 - \mathbf{U}_2\|_{\mathcal{F}}$ for all $t > 0$ and for all $\mathbf{U}_1, \mathbf{U}_2$ in \mathcal{F} .
- $\mathbf{R}(t, \cdot)$ is a compact operator on \mathcal{F} for all $t > 0$.

Proof. It is easy to see from the definition (2.8) of \mathbf{R} that, if it exists, $D^q \mathbf{R}(t, \mathbf{V}_0)[\mathbf{U}_1, \dots, \mathbf{U}_q] = \boldsymbol{\lambda}^q \mathbf{J}(t) \cdot (\mathbf{S}^{(q)}(\boldsymbol{\lambda}(\mathbf{V}_0 - \boldsymbol{\theta})) \cdot (\mathbf{U}_1 \cdots \mathbf{U}_q))$. The notation $\mathbf{U}_1 \cdots \mathbf{U}_q$ is the same as in the definition of $D^q \mathbf{S}$ in equation (2.4), i.e. the component pointwise product of the q functions $\mathbf{U}_1, \dots, \mathbf{U}_q$ of \mathcal{F} .

The q -multilinear operator $D^q \mathbf{R}(t, \mathbf{V}_0)$ is well-defined because, according to corollary 2.1, $\mathbf{U}_1 \cdots \mathbf{U}_q$ is in \mathcal{F} . The first property follows immediately.

It remains to show that the q -multilinear operator $D^q \mathbf{R}(t, \mathbf{V}_0)$ is continuous. We apply corollary 2.1 once more to show that

$$\|D^q \mathbf{R}(t, \mathbf{V}_0) \cdot (\mathbf{U}_1 \cdots \mathbf{U}_q)\|_{\mathcal{F}} \leq \left\| \boldsymbol{\lambda}^q \mathbf{J}(t) \mathbf{S}^{(q)}(\boldsymbol{\lambda}(\mathbf{V}_0 - \boldsymbol{\theta})) \right\|_{\mathcal{F}} \|\mathbf{U}_1 \cdots \mathbf{U}_q\|_{\mathcal{F}} \leq K \prod_i \|\mathbf{U}_i\|_{\mathcal{F}}$$

for some positive constant K , that is $D^q \mathbf{R}$ is continuous and $\mathbf{R}(t, \cdot) \in C^q(\mathcal{F}, \mathcal{F})$.

The second property is proved in [26].

For all α , $|\alpha| \leq m$ $\mathbf{U} \rightarrow \partial^\alpha \mathbf{J} \cdot \mathbf{U}$ are compact operators on $\mathbf{L}^2(\Omega, \mathbb{R}^p)$ because they are Hilbert-Schmidt operators (see [53, chapter X.2]). Hence for any bounded \mathbf{V}_n sequence in \mathcal{F} hence in $\mathbf{L}^2(\Omega, \mathbb{R}^p)$, there exists a subsequence \mathbf{V}'_n such that $D^\alpha \mathbf{J}(t) \cdot \mathbf{S}(\boldsymbol{\lambda}(\mathbf{V}'_n - \boldsymbol{\theta}))$ are convergent in $\mathbf{L}^2(\Omega, \mathbb{R}^p)$ for $|\alpha| \leq m$. Then $\mathbf{R}(t, \mathbf{V}'_n)$ is convergent in \mathcal{F} because of (2.6). We have proved that $\mathbf{R}(t, \cdot)$ is a compact operator on \mathcal{F} . \square

Following closely [24] we have the following proposition.

PROPOSITION 2.5. *If the following two hypotheses are satisfied:*

1. *The connectivity function \mathbf{J} is in $C(\mathbb{R}^+; \mathbf{W}^{m,2}(\Omega \times \Omega, \mathbb{R}^{p \times p}))$ for the values of m given in proposition 2.2, and bounded, $\|\mathbf{J}(t)\|_{\mathcal{F}} \leq J$, $t \geq 0$,*
2. *the external current \mathbf{I}_{ext} is in $C(\mathbb{R}^+; \mathcal{F})$,*

then for any function \mathbf{V}_0 in \mathcal{F} there is a unique solution \mathbf{V} , defined on \mathbb{R}^+ and continuously differentiable, of the initial value problem (2.1). This solution depends upon $3p$ parameters, the slopes $\boldsymbol{\lambda}$, the thresholds $\boldsymbol{\theta}$ and the diagonal matrix \mathbf{L} .

Even if we have made progress in the formulation of the Neural Field equations, there still remains the unsatisfactory possibility that the membrane potential becomes unbounded as $t \rightarrow \infty$. However this is not the case as shown in the next proposition:

PROPOSITION 2.6. *If the external current is bounded in time $\|\mathbf{I}_{\text{ext}}\|_{\mathcal{F}} \leq I_{\text{ext}}$, for all $t \geq 0$, then the solution of equation (2.7) is bounded for each initial condition $\mathbf{V}_0 \in \mathcal{F}$.*

Proof. Let us define $f : \mathbb{R} \times \mathcal{F} \rightarrow \mathbb{R}^+$ as

$$f(t, \mathbf{V}) \stackrel{\text{def}}{=} \langle -\mathbf{L} \cdot \mathbf{V} + \mathbf{J}(t) \cdot \mathbf{S}(\lambda(\mathbf{V} - \boldsymbol{\theta})) + \mathbf{I}_{ext}(t), \mathbf{V} \rangle_{\mathcal{F}} = \frac{1}{2} \frac{d\|\mathbf{V}\|_{\mathcal{F}}^2}{dt}.$$

We note $\tau_{max} = \max_{i=1, \dots, p} \tau_i$ and notice that

$$f(t, \mathbf{V}) \leq -\frac{1}{\tau_{max}} \|\mathbf{V}\|_{\mathcal{F}}^2 + (J + I_{ext}) \|\mathbf{V}\|_{\mathcal{F}}.$$

Thus, if $\|\mathbf{V}\|_{\mathcal{F}} \geq 2\tau_{max}(J + I_{ext}) \stackrel{\text{def}}{=} R$, $f(t, \mathbf{V}) \leq -2\tau_{max}(J + I_{ext})^2 \stackrel{\text{def}}{=} -\delta < 0$.

Let us show that the open ball of \mathcal{F} of center 0 and radius R , B_R , is stable under the dynamics of equation (2.1). We know that $\mathbf{V}(t)$ is defined for all $t \geq 0$ s and that $f < 0$ on ∂B_R , the boundary of B_R . We consider three cases for the initial condition \mathbf{V}_0 .

If $\mathbf{V}_0 \in B_R$ and set $\tau = \sup \{t \mid \forall s \in [0, t], \mathbf{V}(s) \in \overline{B_R}\}$. Suppose that $\tau \in \mathbb{R}$, then $\mathbf{V}(\tau)$ is defined and belongs to $\overline{B_R}$, the closure of B_R , because $\overline{B_R}$ is closed, in effect to ∂B_R . We also have $\frac{d}{dt} \|\mathbf{V}\|_{\mathcal{F}}^2|_{t=\tau} = f(\tau, \mathbf{V}(\tau)) \leq -\delta < 0$ because $\mathbf{V}(\tau) \in \partial B_R$. Thus we deduce that for $\varepsilon > 0$ and small enough, $\mathbf{V}(\tau + \varepsilon) \in \overline{B_R}$ which contradicts the definition of τ . Thus $\tau \notin \mathbb{R}$ and $\overline{B_R}$ is stable.

Because $f < 0$ on ∂B_R , $\mathbf{V}_0 \in \partial B_R$ implies that $\forall t > 0$, $\mathbf{V}(t) \in B_R$.

Finally we consider the case $\mathbf{V}_0 \in \mathbb{C}\overline{B_R}$. Suppose that $\forall t > 0$, $\mathbf{V}(t) \notin \overline{B_R}$, then $\forall t > 0$, $\frac{d}{dt} \|\mathbf{V}\|_{\mathcal{F}}^2 \leq -2\delta$, thus $\|\mathbf{V}(t)\|_{\mathcal{F}}$ is monotonically decreasing and reaches the value of R in finite time when $\mathbf{V}(t)$ reaches ∂B_R . This contradicts our assumption. Thus $\exists \tau > 0 \mid \mathbf{V}(\tau) \in B_R$. \square

COROLLARY 2.7. *If $\mathbf{V}_0 \notin B_R$ and $T = \inf \{t > 0 \mid \mathbf{V}(t) \notin B_R\}$. Then*

$$T \leq \frac{\|\mathbf{V}_0\|_{\mathcal{F}}^2 - R^2}{2\delta}$$

This proposition shows that $\overline{B_R}$ is an attracting set and that it suffices to study the dynamics within this set to have the long time behavior of the solutions of the Neural Fields Equations.

This attracting set contains the stationary solutions of (2.1), we devote the next section to their study. We quote a result from [26] concerning their stability:

PROPOSITION 2.8. *If the condition*

$$\lambda_m \rho(\mathbf{J}_s) < 1,$$

holds, then every stationary solution of (2.1) is globally asymptotically stable. $\lambda_m = \max \lambda_i$, \mathbf{J}_s is the symmetric part $(\mathbf{J} + \mathbf{J}^)/2$ of the operator \mathbf{J} , and $\rho(\mathbf{J}_s)$ its spectral radius. We define λ_L to be $\rho(\mathbf{J}_s)^{-1}$.*

Similar results hold for the activity-based model (2.5).

2.3. Properties of the set of persistent states . We look at the equilibrium states, noted \mathbf{V}_λ^f , of (2.1), when \mathbf{I}_{ext} and \mathbf{J} do not depend upon the time. Our goal is to estimate their number and, if possible, to compute them numerically, for a given set of parameters.

It is quite demanding to do it at a given point in the parameter space except in some very special cases⁴. We note that when $\lambda = 0$ (or $\mathbf{J} = 0$), the stationary equation is trivially solved.

⁴When the nonlinearity $\mathbf{J} \cdot \mathbf{S}(\lambda(\mathbf{V}_\lambda^f - \boldsymbol{\theta}))$ is small compared to the linear part $\mathbf{L} \cdot \mathbf{V}_\lambda^f$, we know there exists a unique solution and how to compute it efficiently. This was proved in [26].

Hence, we can think of deforming this trivial solution to a solution when $\lambda \neq 0$, $\mathbf{J} \neq 0$. This raises a number of questions. Does such a “manifold” of solutions exist *i.e.* can we link the trivial solution to a solution for any given set of parameters? If yes, are there any other solutions? How do these “manifolds” look globally? These questions concern global properties of the set of solutions (existence of branches, existence of intersection points, connectedness. . .) are difficult to answer. We provide some partial answers in the remainder of the article.

Before going deeper in the analysis, we need to simplify the parameter space. The equilibria, also called bumps, or persistent states, are stationary solutions (independent of time) of

$$0 = -\mathbf{L} \cdot \mathbf{V}_\lambda^f + \mathbf{J} \cdot \mathbf{S}(\lambda(\mathbf{V}_\lambda^f - \boldsymbol{\theta})) + \mathbf{I}_{\text{ext}},$$

We redefine \mathbf{J} as $\mathbf{L}^{-1}\mathbf{J}$, \mathbf{V} as $\mathbf{V} - \boldsymbol{\theta}$ and \mathbf{I}_{ext} as $\mathbf{L}^{-1} \cdot \mathbf{I}_{\text{ext}} - \boldsymbol{\theta}$ and restrict our study to:

$$0 = -\mathbf{V}_\lambda^f + \mathbf{J} \cdot \mathbf{S}(\lambda \mathbf{V}_\lambda^f) + \mathbf{I}_{\text{ext}} \quad (2.9)$$

Still, equation (2.9) contains many parameters such as the ones describing \mathbf{J} and \mathbf{I}_{ext} , or the slopes λ . Which parameters to choose for the continuation method: λ or \mathbf{J} ? We decide to fix \mathbf{J} and control λ for two reasons :

- the stationary solutions are bounded for $\lambda \in \mathbb{R}_+^p$, see proposition 2.9.1 which is not the case when $\|\mathbf{J}\| \rightarrow \infty$. This proves to be useful numerically.
- previous studies usually use a Heaviside nonlinearity which is formally equivalent to our nonlinearity when $\lambda \rightarrow \infty$, varying λ can thus bridge the gap with previous approaches.

As a matter of fact the techniques we are about to expose are applicable to any set of parameters with minor modifications. Hence, we now focus on the influence of the slopes λ on the solutions of (2.1). We make the assumption that they are all equal to λ , $\boldsymbol{\lambda} = \lambda \text{Id}_p$, $\lambda \geq 0$. where Id_p is the $p \times p$ identity matrix. The equation becomes

$$0 = -\mathbf{V}_\lambda^f + \mathbf{J} \cdot \mathbf{S}(\lambda \mathbf{V}_\lambda^f) + \mathbf{I}_{\text{ext}} \stackrel{\text{def}}{=} -F(\mathbf{V}_\lambda^f, \lambda) \quad (2.10)$$

It is clear that when $\lambda = 0$, the stationary equation is trivially solved by

$$\mathbf{V}_0^f \stackrel{\text{def}}{=} \mathbf{J} \cdot \mathbf{S}(0) + \mathbf{I}_{\text{ext}} = \frac{1}{2} \mathbf{J} \cdot \mathbf{1} + \mathbf{I}_{\text{ext}},$$

where $\mathbf{1}$ is the p -dimensional vector with all coordinates equal to 1. Let \mathcal{B}_λ be the set of solutions of equation (2.10) for a given slope parameter λ :

$$\mathcal{B}_\lambda = \{\mathbf{V} \mid F(\mathbf{V}, \lambda) = 0\}$$

We next provide some properties of the sets \mathcal{B}_λ .

PROPOSITION 2.9.

1. *The persistent states satisfy the following inequality*

$$\left\| \mathbf{V}_\lambda^f - \mathbf{V}_0^f \right\|_{\mathcal{F}} \leq \|\mathbf{J}\|_{\mathcal{F}} \sqrt{p|\Omega|S_0 \left(\frac{\lambda^2 B_1^2}{p|\Omega|} \right)}, \text{ where } B_1 \stackrel{\text{def}}{=} \sqrt{p|\Omega|} \|\mathbf{J}\|_{\mathcal{F}} + \|\mathbf{I}_{\text{ext}}\|_{\mathcal{F}}$$

where $S_0 : \mathbb{R} \rightarrow \mathbb{R}$ is the “shifted” sigmoid defined by $S_0(x) = S(x) - S(0)$ and the constant B_1 is defined in proposition D.2 of appendix D.1.

2. If the condition

$$\lambda \|\mathbf{J}\|_{\mathcal{F}} < 1 \quad (2.11)$$

is satisfied, then $\#\mathcal{B}_\lambda = 1$. We define λ^* to be $\|\mathbf{J}\|_{\mathcal{F}}^{-1}$.

3. $\forall \lambda \in \mathbb{R}^+$, $\mathcal{B}_\lambda \neq \emptyset$,

4. If the number of solutions in \mathcal{B}_λ is finite, then it must be odd.

5. Let $0 \leq a < b$ be two reals, and consider the set $\mathcal{B} = \cup_{\lambda \in [a, b]} \mathcal{B}_\lambda \times \{\lambda\}$. Then \mathcal{B} contains a connected component \mathcal{C} which intersects $\mathcal{B}_a \times \{a\}$ and $\mathcal{B}_b \times \{b\}$.

Proof.

1. From lemma D.1 in appendix D.1 we have $S_0(\lambda V_{\lambda i}^f)^2 \leq S_0(\lambda^2 (V_{\lambda i}^f)^2)$, $i = 1, \dots, p$. Therefore

$$\sum_{i=1}^p S_0(\lambda V_{\lambda i}^f)^2 \leq \sum_{i=1}^p S_0(\lambda^2 (V_{\lambda i}^f)^2) \leq p S_0\left(\frac{\lambda^2}{p} \sum_{i=1}^p (V_{\lambda i}^f)^2\right).$$

The second inequality comes from Jensen's and the fact that $S_0(\cdot)$ is concave in \mathbb{R}^+ . It then follows, using again Jensen's inequality and the fact that \mathbf{S}_0 is monotonously increasing, that

$$\left\| \mathbf{S}_0(\lambda \mathbf{V}_\lambda^f) \right\|_{\mathbf{L}^2(\Omega, \mathbb{R}^p)}^2 \leq p |\Omega| S_0\left(\frac{\lambda^2}{p |\Omega|} \left\| \mathbf{V}_\lambda^f \right\|_{\mathbf{L}^2(\Omega, \mathbb{R}^p)}^2\right) \leq p |\Omega| S_0\left(\frac{\lambda^2}{p |\Omega|} \left\| \mathbf{V}_\lambda^f \right\|_{\mathcal{F}}^2\right)$$

Now

$$\begin{aligned} \left\| \mathbf{V}_\lambda^f - \mathbf{V}_0^f \right\|_{\mathcal{F}}^2 &= \left\| \mathbf{J} \cdot \mathbf{S}_0(\lambda \mathbf{V}_\lambda^f) \right\|_{\mathcal{F}}^2 = \sum_{|\alpha|=0}^m \left\| D^\alpha \mathbf{J} \cdot \mathbf{S}_0(\lambda \mathbf{V}_\lambda^f) \right\|_{\mathbf{L}^2(\Omega, \mathbb{R}^p)}^2 \\ &\leq \left\| \mathbf{S}_0(\lambda \mathbf{V}_\lambda^f) \right\|_{\mathbf{L}^2(\Omega, \mathbb{R}^p)}^2 \sum_{|\alpha|=0}^m \left\| D^\alpha \mathbf{J} \right\|_{\mathbf{L}^2(\Omega, \mathbb{R}^p)} \leq \left\| \mathbf{S}_0(\lambda \mathbf{V}_\lambda^f) \right\|_{\mathbf{L}^2(\Omega, \mathbb{R}^p)}^2 \|\mathbf{J}\|_{\mathcal{F}}^2 \end{aligned} \quad (2.12)$$

The inequality then follows from proposition D.2.

2. Use the Picard Theorem. As shown in figure 2.2, this imposes that $\lambda^* \leq \lambda_L$. Indeed, as $\rho(\mathbf{J}_s) \leq \|\mathbf{J}_s\|$ and $\|\mathbf{J}_s\| = \|\mathbf{J}\|$, and $\|\mathbf{J}\| \leq \|\mathbf{J}\|_{\mathcal{F}}$, we have $\lambda^* = \|\mathbf{J}\|_{\mathcal{F}}^{-1} \leq \lambda_L = \rho(\mathbf{J}_s)^{-1}$.

3. The first property is that it is non empty: in [26] we proved that persistent states always existed in $\mathbf{L}^2(\Omega, \mathbb{R}^p)$ for all positive values of λ . However, our ambient functional space is different since we require more space regularity. Let us consider a persistent state $\mathbf{V}_\lambda^f \in \mathbf{L}^2(\Omega, \mathbb{R}^p)$ given by [26]. It satisfies $\mathbf{V}_\lambda^f = \mathbf{R}(\mathbf{V}_\lambda^f)$. But $\mathbf{R} : \mathbf{L}^2(\Omega, \mathbb{R}^p) \rightarrow \mathcal{F}$ because of the assumptions on $\mathbf{J}(\mathbf{r}, \mathbf{r}')$ and \mathbf{I}_{ext} . Hence any persistent state in $\mathbf{L}^2(\Omega, \mathbb{R}^p)$ in fact belongs to \mathcal{F} .

4. Suppose that \mathcal{B}_λ has an infinite number of solutions, then the proposition holds. If now, \mathcal{B}_λ has a finite number of solutions, we can assume that these points are non critical. Then according to the Leray-Schauder degree theory sketched in appendix B we have

$$\begin{aligned} \deg_{\text{LS}}(F(\mathbf{V}, \lambda), B_r, 0) &= \sum_{\mathbf{V}_\lambda^f \in \mathcal{B}_\lambda} \text{sign det}_{\text{LS}}(D_V F(\mathbf{V}_\lambda^f, \lambda), B_r, 0) = \\ &= \sum_{\mathbf{V}_\lambda^f \in \mathcal{B}_\lambda} \text{sign det}_{\text{LS}}(\text{Id} - \lambda \mathbf{J} \mathbf{D} \mathbf{S}(\lambda \mathbf{V}_\lambda^f)), \end{aligned}$$

where $r = 2B_1$ and B_1 is defined in proposition D.2 in appendix D.1. We prove in corollary B.2 in appendix B that the first term is equal to 1. Suppose now that \mathcal{B}_λ contains an even number of points, say $2k$ among which l correspond to a negative sign and hence $2k - l$ to a positive sign. The sum that appears in the last term is equal to $2k - 2l$, hence even. Hence \mathcal{B}_λ must possess an odd number of points.

5. The proof uses the Leray-Schauder theorem, see appendix B. We apply the theorem to the function $F : \mathcal{F} \times J \rightarrow \mathcal{F}$ which is of the form $\text{Id} + m$, with $m(\cdot) = -\mathbf{R}$. Because m is compact on $\mathcal{F} \times J$ (see proof in [24]), $\mathcal{B}_a \times \{a\}$ bounded, and there exists an open bounded neighbourhood \mathcal{U}_a of \mathcal{B}_a such that $\deg_{\text{LS}}(F(\cdot, a), \mathcal{U}_a, 0) \neq 0$ (corollary B.2 in appendix B), the conclusion follows since the connected component cannot be unbounded, \mathcal{B} being bounded.

□

This proposition answers some of the previous questions. For any positive value of λ , there is always at least one persistent state and we can find a way to connect the trivial solution \mathbf{V}_0^f to a persistent state corresponding to an arbitrary value of the parameter λ . We return to this connection later. All this is true if we choose, say $\|\mathbf{J}\|_{\mathcal{F}}$, as a parameter instead of λ . We will also see that not all the solutions in \mathcal{B}_λ are in the connected component of $(\mathbf{V}_0^f, 0)$ in $\mathcal{F} \times \mathbb{R}_+$.

Regarding the connection between \mathbf{V}_0^f and \mathbf{V} , proposition 2.9 does not give us any indication on its regularity but we have the following corollary.

COROLLARY 2.10. *Let a and b be as in proposition 2.9. For all $\varepsilon > 0$ there exists a finite sequence $(\mathbf{V}_1, \lambda_1), \dots, (\mathbf{V}_n, \lambda_n)$ of points of \mathcal{C} such that $\|\mathbf{V}_i - \mathbf{V}_{i+1}\|_{\mathcal{F}} \leq \varepsilon$ for $i = 1, \dots, n-1$ and $\lambda_1 = a, \lambda_n = b$.*

Proof. \mathcal{C} is connected for any topology equivalent to the product topology of $\mathcal{F} \times [a, b]$, e.g. for the metric defined by $d((\mathbf{V}_1, \lambda_1), (\mathbf{V}_2, \lambda_2)) = \|\mathbf{V}_1 - \mathbf{V}_2\|_{\mathcal{F}} + |\lambda_1 - \lambda_2|$. Since it is connected for this metric, it is also well-chained [14], and the conclusion follows. □

In fact, except at points where the Jacobian of F is non-invertible (such points like B in figure 2.1 are potential bifurcation points), the implicit functions theorem tells that $\lambda \rightarrow (\mathbf{V}_\lambda^f, \lambda)$ is differentiable. Hence in effect proposition 2.9.5 imposes strong constraints on the set \mathcal{B}_λ as shown in figure 2.1. The horizontal axis represents the parameter λ , the vertical axis the space \mathcal{F} where the solutions of (2.10) live. The curves represent possible solutions as functions of λ . The configuration in the lefthand part of the figure are forbidden by proposition 2.9.5 while those on the righthand side are allowed, the green curve being an example of a continuous curve $s \rightarrow (\mathbf{V}_{\lambda(s)}^f, \lambda(s))$ from $[0, 1]$ to $\mathcal{F} \times [a, b]$.

Proposition 2.9.5 gives a very interesting general (non-local) property of the set of solutions. But it is non-constructive, for example it does not tell us which branch to chose at point B in figure 2.1 and we need to compute all the branches to know the path to $\lambda = b$. Hopefully such branching points as B are very rare and one only sees turning points rather than branching points (such as the one at λ_1 in figure 2.2, left): any perturbation will indeed destroy such branching points (see figure 2.2 right). Hence, if one continues the trivial solution (obtained for $\lambda = 0$), one will typically find a curve like the green one in figure 2.2.Right. This may lead to the wrong conclusion that for λ big enough there is only one stationary solution instead of three. The problem is to find a way to compute, if it exists, the second, red, curve which is not connected to the green curve, hence not attainable by λ -continuation.

An idea, directly suggested by the above picture is to restore the branching points by

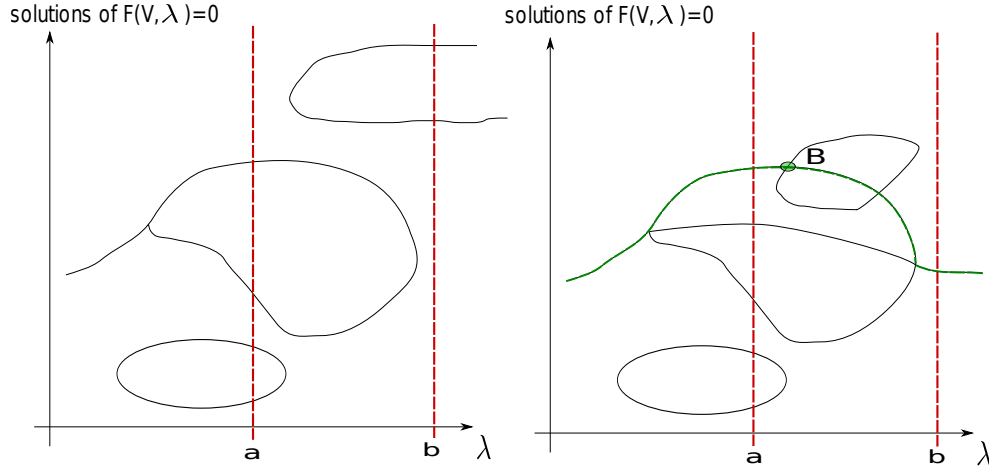


FIG. 2.1. In the lefthand part of the figure, there is no connected curve of solutions in $[a, b]$: this is forbidden by proposition 2.9.5 which states that we must be in the situation shown in the righthand part of the figure, where the green curve connects $\mathcal{B}_a \times \{a\}$ and $\mathcal{B}_b \times \{b\}$, see text.

perturbation. Among all possible perturbations, we choose one of the simplest, i.e. we vary the amplitude of the external input \mathbf{I}_{ext} . Hence we define the external current \mathbf{I}_{ext} to be $\varepsilon \mathbf{I}_{\text{ext}}$ where the contrast ε satisfies $0 \leq \varepsilon \leq 1$. This is suggested by experimentalists who usually provide neural responses as functions of the contrast. Note that some non-generic external input may not break the branching points (see section 3.2).

The conclusion is that if we want one solution for $\lambda \neq 0$, we use a λ -continuation of the trivial solution, but if we want more than one (or the maximum number of) solutions for $\lambda \neq 0$, then we perform a (λ, ε) -continuation of the trivial solution.

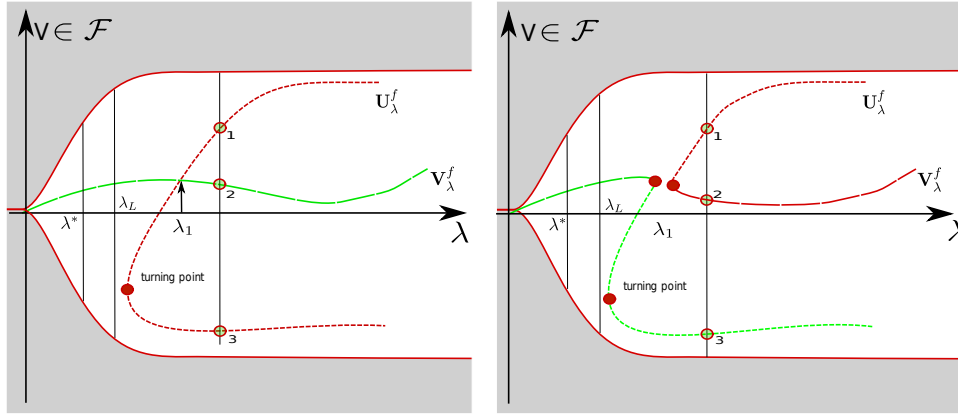


FIG. 2.2. The white zone is the domain of existence of \mathbf{V}^f . The grey zone is excluded thanks to proposition 2.9.1. Left: non generic situation, a transcritical bifurcation occurs at λ_1 . Right: same as left with a small perturbation (like a tiny change of the external input \mathbf{I}_{ext}), the transcritical bifurcation has opened up. λ_L is defined in prop.2.8 and λ^* in prop.2.9.

Remark 2. An interesting question is to predict how close to λ_L can be the smallest value of λ where a “turning point” occurs.

However, when performing this (λ, ε) -continuation of the trivial solution, we may end-up with a lot of data. Hence, we need to have an idea of the structure of the set $(\mathbf{V}_{\lambda, \varepsilon}^f, \lambda, \varepsilon)$. The idea is, again, to think of this set as a deformation of an easier to compute set of stationary solutions. This is done in the next section.

Remark 3. It is highly possible that this (λ, ε) -continuation scheme still misses some solutions. One possibility is to introduce a third parameter, but it may become quickly numerically untractable.

3. Exploring the set of persistent states. We exploit the fact that in the neural field equation (2.10) the ratio between the external current \mathbf{I}_{ext} and \mathbf{J} is not fixed a priori. Hence when studying the NFE, one would rather look at

$$-\mathbf{V} + \mathbf{J} \cdot \mathbf{S}(\lambda \mathbf{V}) + \varepsilon \mathbf{I}_{ext} = 0 \quad (3.1)$$

where $\varepsilon \geq 0$. The persistent states now depend upon the pair (λ, ε) i.e. $\mathbf{V}_{\lambda, \varepsilon}^f$. The idea is to infer the persistent states of (3.1) from those, $\mathbf{V}_{\lambda, 0}$ of

$$-\mathbf{V} + \mathbf{J} \cdot \mathbf{S}(\lambda \mathbf{V}) = 0 \quad (3.2)$$

We further simplify the problem by considering

$$-\mathbf{V} + \mathbf{J} \cdot \mathbf{S}_0(\lambda \mathbf{V}) + \mu \mathbf{J} \cdot \mathbf{S}(0) = 0, \quad (3.3)$$

where \mathbf{S}_0 is defined in proposition 2.9. We recover equation (3.2) when $\mu = 1$. The advantage is that when $\mu = 0$, we can say a great deal about the persistent states.

3.1. A simpler case. This simpler case reduces to the study of the previous equation when $\mu = 0$:

$$-\mathbf{V} + \mathbf{J} \cdot \mathbf{S}_0(\lambda \mathbf{V}) = 0 \quad (3.4)$$

In other words, we infer the persistent states of (3.1) from those, $\mathbf{V}_{\lambda, \varepsilon=0, \mu=0}$ of equation (3.4). This case has been studied a lot by several authors [20, 16, 8] when a constant current \mathbf{I}_{ext} is applied, which amounts to changing the threshold θ in \mathbf{S} .

$\mathbf{V} = 0$ is a trivial persistent state for (3.4). Remember that a necessary condition for the equation $F(\mathbf{V}, \lambda) = 0$ to bifurcate at the solution $(\mathbf{V}_{\lambda}^f, \lambda)$ is that $D_{\mathbf{V}}F(\mathbf{V}_{\lambda}^f, \lambda)$ is non-invertible.

For technical reasons it is interesting to slightly modify the nonlinear term \mathbf{R} in (2.7) by subtracting from it its linear part as follows. We rewrite (3.4) as

$$\mathbf{L}_{\lambda} \cdot \mathbf{V} + \mathbf{R}(\lambda, \mathbf{V}) = 0 \quad (3.5)$$

with $\mathbf{R}(\lambda, \mathbf{V}) = O(\|\mathbf{V}\|_{\mathcal{F}}^2)$ and

$$\mathbf{L}_{\lambda} = -\text{Id} + \lambda \mathbf{J} \mathbf{D} \mathbf{S}_0(0) = -\text{Id} + \frac{\lambda}{4} \mathbf{J} \quad (3.6)$$

The operator \mathbf{L}_{λ} satisfies the following properties.

PROPOSITION 3.1.

- The operator \mathbf{J} is a compact linear operator on \mathcal{F} .
- $\mathbf{L}_{\lambda} = -\text{Id} + \frac{\lambda}{4} \mathbf{J}$ is a Fredholm operator of index 0 (useful for static bifurcation, see [30]).
- \mathbf{L}_{λ} is a sectorial operator (useful for dynamical bifurcation, see [30]).

Proof. The first property was proved in lemma 2.4.

Because \mathbf{J} is a compact operator, the kernel of $-\text{Id} + \frac{\lambda}{4}\mathbf{J}$ is of finite dimension equal to the codimension of its image, hence its index is 0.

\mathbf{L}_λ is a sectorial operator because it is a bounded linear operator on a Banach space, see e.g. [31]. \square

We can therefore state that the values of the parameter λ that determine the *possible* bifurcation points are:

$$\lambda_n = \frac{4}{\sigma_n}, n = 1, 2, \dots \quad (3.7)$$

where σ_n is an eigenvalue of the compact operator \mathbf{J} . We assume in the sequel that $\lambda_1 \leq \lambda_2 \leq \dots$.

Additional properties have to be met in order to have a bifurcation point (see [41]) but they are satisfied if every eigenvalue of \mathbf{J} is simple. We will assume that the first $k \geq 1$ (k is arbitrary) eigenvalues are simple because this class of operators is dense in the set of compact operators set (see [41]). We denote by e_n (respectively by e_n^*) the eigenvector of \mathbf{J} (respectively of the adjoint operator \mathbf{J}^*) for the eigenvalue σ_n .

A simple adaptation of lemma 2.4 shows that \mathbf{R} is C^q , for all integer q and we can consider (if it exists the minimal integer $q \geq 2$ such that

$$0 \neq \chi_q^{(n)} \equiv \langle G_q(e_n, \lambda_n), e_n^* \rangle_{\mathcal{F}}.$$

According to lemma 2.4

$$G_q(e_n, \lambda_n) = \frac{1}{q!} D^q \mathbf{R}(\lambda_n, \mathbf{0})[e_n \cdots e_n] = \frac{\lambda_n^q}{q!} S_0^{(q)}(0) \mathbf{J} \cdot (e_n \cdots e_n)$$

By parity, $S_0^{(q)}(0) \stackrel{\text{def}}{=} s_q \neq 0$ if and only if q is odd. Hence, the parity of q , which is odd, tells that we have a pitchfork bifurcation at λ_n . In particular, the bifurcated branch is given by

$$\mathbf{V}_\lambda^f = x(\lambda)e_n + o(x)$$

Thus the bifurcation portrait is a set of branches \mathcal{C}_n emanating at points (at least for $n \leq k$) $(0, \lambda_n)$. Thanks to proposition.3.1, we can apply the Lyapunov-Schmidt procedure (see [30]) to get the following reduced equation on $x \in \mathbb{R}$:

$$0 = (-1 + \lambda\sigma_n/4)x + g(x, \lambda) = (-1 + \lambda\sigma_n/4)x + \chi_q^{(n)}x^q + o(x^q)$$

Depending on the sign of $\chi_q^{(n)}$, the pitchfork branch is oriented toward $\lambda < \lambda_n$ (resp. $\lambda > \lambda_n$) if $\chi_q^{(n)} > 0$ (resp. $\chi_q^{(n)} < 0$). Let us note e_n^q the vector $\underbrace{e_n \cdots e_n}_{q \text{ times}}$. We have

$$\chi_q^{(n)} = \frac{\lambda_n^q s_q}{q!} \langle \mathbf{J} \cdot e_n^q, e_n^* \rangle_{\mathcal{F}} = \frac{\lambda_n^q s_q}{q!} \langle e_n^q, \mathbf{J}^* \cdot e_n^* \rangle_{\mathcal{F}} = \frac{\lambda_n^{q-1} s_q}{q! s_1} \langle e_n^q, e_n^* \rangle_{\mathcal{F}}$$

From a practical standpoint, the last inner product is difficult to compute since it requires the computation of the eigenvectors of the adjoint operator \mathbf{J}^* of \mathbf{J} for the inner-product of the Hilbert space $\mathcal{F} = \mathbf{W}^{m,2}$ which are in general different from those of the adjoint operator

\mathbf{J}_2^* of \mathbf{J} for the inner-product of the Hilbert space $\mathbf{W}^{0,2} \equiv \mathbf{L}^2$. This computation is greatly simplified by the following proposition.

PROPOSITION 3.2. *Let $e_{L^2}^*$ be an eigenvector of the adjoint operator $\mathbf{J}_{L^2}^*$ of \mathbf{J} for the inner-product of the Hilbert space \mathbf{L}^2 , associated to the eigenvalue λ (assumed to be simple). Let $e_{\mathcal{F}}^*$ be the corresponding eigenvector of the adjoint operator $\mathbf{J}_{\mathcal{F}}^*$ of \mathbf{J} for the inner-product of the Hilbert space $\mathcal{F} = \mathbf{W}^{m,2}$. Then it is possible to choose $e_{\mathcal{F}}^*$ such that the following holds*

$$\langle \mathbf{U}, e_{\mathcal{F}}^* \rangle_{\mathcal{F}} = \langle \mathbf{U}, e_{L^2}^* \rangle_2 \quad \forall \mathbf{U} \in \mathcal{F}$$

Proof. see appendix.E. \square

In effect, in order to obtain the sign of $\chi_q^{(n)}$, we only have to compute the eigenvectors of \mathbf{J}_2^* and to compute inner products in \mathbf{L}^2 .

Thus, we have found local branches of stationary solutions and continue them globally in order to obtain the global branches named \mathcal{C}_n . An interesting question, yet unsolved, is to know whether the branches \mathcal{C}_n are connected. Some results exist in that direction in the line of those of Rabinowitz (see [46, 41]) but do not provide much insight in the general case ($d > 1, p > 1 \dots$). However, they can be used to derive some properties of \mathcal{C}_1 .

PROPOSITION 3.3 (Turning point property). *If $\chi_q^{(n)} > 0$, then $\exists \lambda_T < \lambda_1$ such that $\forall \lambda \in (\lambda_T, \lambda_1)$, (3.4) has at least 3 solutions and $\lambda_T = \min \{ \lambda / (\mathbf{V}^f, \lambda) \in \mathcal{C}_1 \}$.*

Proof. Let \mathcal{C}_1 be the connected component in \bar{B} where $B = \{ (\mathbf{V}, \lambda) \mid \mathbf{V} \neq \mathbf{0}, (\mathbf{V}, \lambda) \text{ satisfies (3.4)} \}$ to which $(\mathbf{0}, \lambda_1)$ belongs. Then (see [41]) \mathcal{C}_1 is unbounded in $\mathcal{F} \times \mathbb{R}_+$ or contains a point $(\mathbf{0}, \lambda_n)$, $n > 1$. In either case, \mathcal{C}_1 exists until $\lambda = \lambda_2$.

$\tilde{\mathcal{C}} = \bar{\mathcal{C}}_1 \cap (\mathcal{F} \times [\lambda^*, \lambda_2])$ is closed and bounded (because every solution \mathbf{V}_λ^f is bounded in \mathcal{F}). Let us show that $\tilde{\mathcal{C}}$ is compact in $\mathcal{F} \times [0, \lambda_2]$. Consider a sequence (\mathbf{V}_n, s_n) in $\tilde{\mathcal{C}}$. As s_n is bounded, we can assume it is convergent. We also have $\mathbf{V}_n = \mathbf{J} \cdot \mathbf{S}_0(s_n \mathbf{V}_n)$. As $(\mathbf{V}, \lambda) \rightarrow \mathbf{J} \cdot \mathbf{S}_0(\lambda \mathbf{V})$ is a compact operator, there exists a subsequence $(\mathbf{V}_{\phi(n)}, s_{\phi(n)})$ such that $\mathbf{J} \cdot \mathbf{S}_0(s_{\phi(n)} \mathbf{V}_{\phi(n)})$ is convergent, hence $\mathbf{V}_{\phi(n)}$ is converging. We have proved that $\tilde{\mathcal{C}}$ is compact. Hence $\Pi_{\mathbb{R}^+}(\tilde{\mathcal{C}})$ is a compact subset of \mathbb{R}^+ . Then $\inf \Pi_{\mathbb{R}^+}(\tilde{\mathcal{C}})$ is a *min* written $\lambda_T \in \Pi_{\mathbb{R}^+}(\tilde{\mathcal{C}})$. As it is an inf, there exists a sequence s_n associated to a \mathbf{V}_n in $\tilde{\mathcal{C}}$ such that $s_n \rightarrow \lambda_T$. But as $\tilde{\mathcal{C}}$ is compact, we can assume that $\mathbf{V}_n \rightarrow \mathbf{V}_T$. Then $(\mathbf{V}_T, \lambda_T) \in \mathcal{C}$ is called a *turning point*⁵.

So we have proved that $\lambda_T \leq \lambda_1$. But in the case q odd with $\chi_q^{(n)} > 0$, \mathcal{C}_1 exists for $\lambda < \lambda_1$ and $\lambda_T < \lambda_1$.

Now, $\forall \lambda \in (\lambda_T, \lambda_1)$, $\exists (\mathbf{V}_\lambda^f, \lambda) \in \mathcal{C}_1 \setminus \{(\mathbf{0}, \lambda)\}$ because \mathcal{C}_1 intersects $\{\mathbf{0}\} \times \mathbb{R}_+$ only at bifurcation points $(\mathbf{0}, \lambda_n)$ located 'after' λ_1 . Then because of proposition 2.9 part 4, there are at least three solutions. \square

Remark 4. *If the sigmoidal function had satisfied $S^{(2)}(0) \neq 0$, we would have seen transcritical bifurcations and the previous proposition still holds in that case.*

Remark 5. *If we were able to prove that the branches do not intersect, the previous proposition would apply to all branches \mathcal{C}_n satisfying the required conditions.*

Even if we do not deal with the dynamics, we can say a little using [30, 41, 38]. At every bifurcation point, the center manifold at $\mathbf{V} = 0$ (see [30]) is one-dimensional while the dimension of the unstable manifold increases as λ crosses values corresponding to transcritical

⁵Not in the sense of [38], here it denotes a local extremum in the parameter along the curve of solutions.

points. Hence for large λ s, we can have a large unstable manifold. Note that every value of λ is biologically plausible because the locally (around $\mathbf{V} = 0$) exponentially divergent dynamic is bounded (see proposition 2.6), which can make the “global” dynamics **very** intricate. In effect, when λ grows to infinity, the sigmoid tends to a Heaviside function which acts as a threshold.

Remark 6. Note that it is easy to characterize Breathers (see [43, 18]) in this framework. It is sufficient to choose a connectivity function \mathbf{J} with complex eigenvalues. For example with a model of two populations ($p = 2$), one excitatory, one inhibitory, such that:

$$\mathbf{J}(\mathbf{r}, \mathbf{r}') = \begin{bmatrix} G_1(\mathbf{r}, \mathbf{r}') & -G_2(\mathbf{r}, \mathbf{r}') \\ G_2(\mathbf{r}, \mathbf{r}') & G_1(\mathbf{r}, \mathbf{r}') \end{bmatrix} \quad G_i \text{ symmetric } \geq 0, [G_1, G_2] = 0$$

Then $\sigma(\mathbf{J}) = \{g_{1,n} \pm ig_{2,n}, g_{i,n} \in \sigma(G_i)\}$ and a Hopf bifurcation occurs at $\lambda_{H,n} = \frac{1}{2S'(0)g_{1,n}}$ if the eigenvalue is simple. Because \mathbf{R} is C^3 , we can also compute its first Lyapunov coefficient (see [30],[38]p.107) and find

$$l_1 = -\frac{\lambda_{H,n}^3 s_2^2}{4\omega_n^2 s_1} \left(1 - \sqrt{g_{1,n}^2 + g_{2,n}^2} \frac{s_3 s_1}{s_2^2} \right)$$

with $\omega_n = \frac{\sqrt{g_{1,n}^2 + g_{2,n}^2}}{2g_{1,n}}$, $s_2 = S^{(2)}(0)$, $s_3 = S^{(3)}(0)$

3.1.1. The case $d = 1, p = 1$. We can use the results of Rabinowitz (see [46]) in the case $d = p = 1$ and when the connectivity operator \mathbf{J} is a symmetric convolution. In that case the zeros of the eigenstates of \mathbf{J} are simple on $\Omega \subset \mathbb{R}$ (because they are cos and sin functions). Moreover the Taylor formula allows to write $\mathbf{S}_0(x) = xh(x)$ with $h > 0$. Then from [46], it follows that the bifurcated branches⁶ \mathcal{C}_n (pitchfork or transcritical) meet $(\lambda_n, 0)$ and ∞ and are characterized by the number of zeros of their elements ; namely $\forall (\mathbf{V}^f, \lambda) \in \mathcal{C}_n$, \mathbf{V}^f has exactly $n - 1$ zeros in Ω . As a consequence, the branches \mathcal{C}_n do not intersect.

If we were able to prove that all the stationary solutions are connected to the zero solution, we would have completely characterized \mathcal{B} . Nevertheless, it is still a lot of information.

Remark 7. The study of the simpler case is very important for the numerics. Indeed, it allows analytical predictions. When one performs the (λ, μ, ϵ) -continuation, one should look at the section of solutions $(\lambda, \mu = 0, \epsilon = 0)$ and compare to the predictions of the simpler case to see if the numerical did not miss some solutions (that may happen when the system has some symmetries).

3.2. Returning to the original equation. The overall picture that emerges from the previous section is interesting despite the fact that some of its features are hard to justify from the biological viewpoint: no external input, rate function \mathbf{S}_0 possibly negative. The reason is that it gives clues about the set of persistent states when $\epsilon \neq 0$ and provides a way to compute them numerically. Starting with the trivial solution \mathbf{V}_0^f of (3.2) when the slope parameter λ is null, we can perform a numerical continuation with respect to the two parameters λ, ϵ .

When $\epsilon \neq 0$, the only bifurcations that are possibly unaltered are the turning points. The transcritical/pitchfork bifurcations will be “opened” as described below. We are still able to predict the stability near the points $(\mathbf{0}, \lambda_n)$. Let us note $\bar{I} = \langle \mu \mathbf{J} \cdot \mathbf{S}(0) + \epsilon \mathbf{I}_{ext}, e_n^* \rangle_{\mathcal{F}}$. Then, the Lyapunov-Schmidt method [30, 41] leads to

$$0 = \left(-1 + \frac{\lambda \sigma_n}{4}\right)x + \chi_q^{(n)} x^q + \bar{I} + o(x^q) \quad (3.8)$$

⁶Here they are connected components in $C^1(\Omega, \mathbb{R}) \times \mathbb{R}_+$ rather than in $\mathcal{F} \times \mathbb{R}_+$.

Notice that when $q = 2$, we find the same equilibria as those of the Bogdanov-Takens normal form and for $q = 3$, we obtain a cusp. Solving the polynomial equation (3.8) allows us to describe different opening scenarios depending on the sign of \bar{I} . The cases $\bar{I} > 0$ are shown on figure 3.1. The case of λ_1 is a little bit special according to proposition 3.3 and is shown in the righthand part of figure 3.1. Note that if $\bar{I} = 0$, a non generic situation, the pitchfork bifurcations are not opened by the addition of the external current.

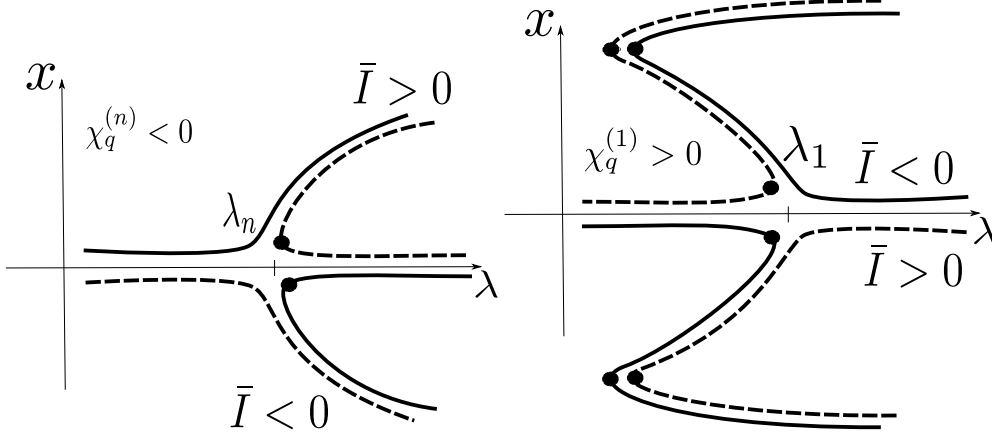


FIG. 3.1. Opening of the pitchfork bifurcation at the first (right) and n th ($n > 1$, left) eigenvalue. Black dots indicate saddle nodes. Note that there are three such points, see proposition 3.3, for the first eigenvalue. Note that the branch may have a more intricate shape than the one shown.

Remark 8. When the first eigenvalue generates a 'well oriented' pitchfork branch, proposition 3.3 says that a turning point must occur on this branch: there are two turning points on this branch. Still we have a local description and it would be interesting to have more global results for example concerning the behavior of these turning points when (λ, ε) varies.

4. Reduction to a finite dimensional analysis. Neural field models are one of the possible generalizations of standard neural networks considered as discrete sets of connected neurons. They can be characterized by two limit processes. First, we let the total number of neurons grow to infinity so that each node of the network represents an ideally infinite number of neurons, in practice a large number of such neurons belonging to different populations, in effect a neural mass. Second, we assume that these neural masses form a continuous neural material and let the connectivity graph of the neural network become continuous. The graph connectivity matrix then turns into a continuous function of the spatial coordinates. One would think that after passing twice to the limit the resulting system would be infinite-dimensional. However, the dimensionality of the neural field models depends essentially upon the linear operator \mathbf{J} representing the connectivity function. If this linear operator has a finite-dimensional range, we show below that the corresponding neural field model is finite-dimensional and is equivalent to a finite set of ordinary differential equations. Moreover, even if this condition is not met we also show that we can always approximate the operator as accurately as desired by a finite-dimensional range operator and reduce the neural field model to a finite set of ordinary differential equations.

4.1. The Pincherle-Goursat Kernels. In our numerical studies we use connectivity functions that are such that the corresponding linear operators of \mathcal{F} have finite rank, i.e. their

range is a finite dimensional subspace of \mathcal{F} . This is without loss of generality because of the following theorem (see, e.g. [13]):

THEOREM 4.1. *The subspace $\mathcal{R}_f(\mathcal{F})$ of finite-dimensional range linear operators of \mathcal{F} is dense in \mathcal{H} , the set of linear compact operators of \mathcal{F} .*

Proof. This is true because \mathcal{F} is a Hilbert space [13, Chapter 6] \square

In the area of integral equations, these operators are called Pincherle-Goursat kernels [50], in short PG-kernels. They are defined as follows

DEFINITION 4.2 (Pincherle-Goursat Kernels). *The connectivity kernel $\mathbf{J}(\mathbf{r}, \mathbf{r}')$ is a PG-kernel if*

$$\mathbf{J}(\mathbf{r}, \mathbf{r}') = \sum_{k=1}^N X_k(\mathbf{r}) \otimes Y_k(\mathbf{r}')$$

where $X_k, Y_k, k = 1 \dots N$ are two sets of N linearly independent elements of \mathcal{F} , and $X_k(\mathbf{r}) \otimes Y_k(\mathbf{r}')$ is the rank 1 $p \times p$ matrix $X_k(\mathbf{r})Y_k^T(\mathbf{r}')$.

We have

$$\mathbf{J} \cdot \mathbf{U} = \sum_k X_k \langle Y_k, \mathbf{U} \rangle_2,$$

where $\langle \cdot, \cdot \rangle_2$ is a short notation for the inner-product in $\mathbf{L}^2(\Omega, \mathbb{R}^p)$. Thus $\mathbf{J} \cdot \mathbf{U} \in \text{Span}(X_1, \dots, X_N)$ which we denote by $R(\mathbf{J})$.

4.2. Persistent state equation for PG-kernels. We now cast the problem of the computation of the solutions of equation (2.10) into the PG-kernel framework:

$$\mathbf{V} - \mathbf{I}_{\text{ext}} = \mathbf{J} \cdot \mathbf{S}(\lambda \mathbf{V})$$

Since $\mathbf{V} - \mathbf{I}_{\text{ext}} \in R(\mathbf{J})$, we can write $\mathbf{V} - \mathbf{I}_{\text{ext}} = \sum_k v_k X_k$, and note $v = (v_k)_{k=1 \dots N}$. The persistent state equation reads:

$$v_k = \left\langle Y_k, \mathbf{S} \left(\lambda \left(\sum_k v_k X_k + \mathbf{I}_{\text{ext}} \right) \right) \right\rangle_2 \quad k = 1, \dots, N$$

This is a set of N nonlinear equations in the N unknowns v_1, \dots, v_N which can be solved numerically using classical methods.

4.3. Reduction to a finite number of ordinary differential equations. In this section we reduce equation (2.1) (when \mathbf{J} is independent of t) to a system of ODEs. We write \mathbf{I} instead of \mathbf{I}_{ext} for simplicity and note \mathbf{S}_λ the function $\mathbb{R}^p \rightarrow \mathbb{R}^p$ defined by $\mathbf{S}_\lambda(x) = \mathbf{S}(\lambda x)$ for $x \in \mathbb{R}^p$.

We note $R(\mathbf{J})^\perp$ the orthogonal complement of $R(\mathbf{J})$ in \mathcal{F} with respect to the inner-product $\langle \cdot, \cdot \rangle_2$:

$$\mathcal{F} = R(\mathbf{J}) \oplus R(\mathbf{J})^\perp$$

We write

$$\mathbf{V} = \mathbf{V}^\parallel + \mathbf{V}^\perp,$$

where \mathbf{V}^\parallel (resp. \mathbf{V}^\perp) is the orthogonal projection of \mathbf{V} on $R(\mathbf{J})$ (resp. $R(\mathbf{J})^\perp$). We have a similar decomposition for the external current \mathbf{I}

$$\mathbf{I} = \mathbf{I}^\parallel + \mathbf{I}^\perp$$

We now decompose $R(\mathbf{J})$ as a Cartesian product of p finite dimensional subspaces of \mathcal{G} . Because

$$\mathbf{J}_{ij}(\mathbf{r}, \mathbf{r}') = \sum_{k=1}^N X_k^i(\mathbf{r}) Y_k^j(\mathbf{r}') \quad i, j = 1, \dots, p,$$

each coordinate $V_i, i = 1, \dots, p$ of \mathbf{V} satisfies

$$\dot{V}_i + \alpha_i V_i = \sum_{k=1}^N \langle Y_k, \mathbf{S}(\lambda \mathbf{V}) \rangle_2 + I_i \quad i = 1, \dots, p$$

Let us consider the p finite dimensional subspaces $E_i, i = 1, \dots, p$ of \mathcal{G} , where each E_i is generated by the N elements $X_k^i, k = 1, \dots, N$. We note E_i^\perp the orthogonal complement of E_i in \mathcal{G} . This induces a decomposition of \mathcal{F} as the direct sum of the cartesian product $\prod_{i=1}^p E_i = R(\mathbf{J})$ and its orthogonal complement $\prod_{i=1}^p E_i^\perp = R(\mathbf{J})^\perp$. We write $V_i = V_i^\parallel + V_i^\perp$ as well as $I_i = I_i^\parallel + I_i^\perp$. We then have

$$\begin{cases} \dot{V}_i^\parallel + \alpha_i V_i^\parallel = \sum_{k=1}^N \langle Y_k, \mathbf{S}(\lambda \mathbf{V}) \rangle_2 + I_i^\parallel \\ \dot{V}_i^\perp + \alpha_i V_i^\perp = I_i^\perp \end{cases} \quad i = 1, \dots, p \quad (4.1)$$

Considering the canonical basis $e_i, i = 1, \dots, p$, of \mathbb{R}^p , we define

$$\begin{aligned} \mathbf{V}^\parallel &= \sum_{i=1}^p V_i^\parallel e_i & \mathbf{I}^\parallel &= \sum_{i=1}^p I_i^\parallel e_i \\ \mathbf{V}^\perp &= \sum_{i=1}^p V_i^\perp e_i & \mathbf{I}^\perp &= \sum_{i=1}^p I_i^\perp e_i \end{aligned}$$

We obtain the $2p$ -dimensional non-autonomous system of ODEs:

$$\begin{cases} \dot{\mathbf{V}}^\parallel + \mathbf{L} \cdot \mathbf{V}^\parallel = \mathbf{J} \cdot \mathbf{S}(\lambda \mathbf{V}) + \mathbf{I}^\parallel \\ \dot{\mathbf{V}}^\perp + \mathbf{L} \cdot \mathbf{V}^\perp = \mathbf{I}^\perp \end{cases} \quad (4.2)$$

Remark 9. If \mathbf{I}^\perp is stationary then \mathbf{V}^\perp converges to $\mathbf{L}^{-1} \mathbf{I}^\perp$.

5. One population of orientation tuned neurons: the ring model. As an application of the previous results, we study the ring model of orientation tuning introduced by Hansel and Sompolinski (see [29, 49, 20, 19, 10, 12]), after the work of Ben-Yishai (see [4]), as a model of a hypercolumn in primary visual cortex. It can be written as:

$$\tau \dot{A}(x, t) = -A(x, t) + S \left(\lambda \left(\int_{-\pi/2}^{\pi/2} J(x-y) A(y, t) dy / \pi + I(x) - \theta \right) \right)$$

Some authors, [10, 12], chose J to be a difference of Gaussians. On the other hand, Ben-Yishai, in [4], started with a network of excitatory/inhibitory spiking neurons and derived a meanfield approximation of this network yielding the activity response described by the following equations:

$$\begin{cases} \tau \dot{A}(x, t) = -A(x, t) + S \left(\lambda \left(\int_{-\pi/2}^{\pi/2} [J_0 + J_1 \cos(\alpha(y-x))] A(y, t) dy / \pi + \varepsilon I(x) - \theta \right) \right) \\ I(x) = 1 - \beta + \beta \cos(\alpha(x-x_0)) \end{cases} \quad (5.1)$$

$\alpha = 2$, $0 \leq \beta \leq 1$ and the threshold $\theta = 1$ in the above cited papers. Being an activity model and not a voltage model in the terminology of [20, 24] it is not directly amenable to our analysis. We can either extend this analysis to activity models as shown in appendix D or do the following. We rewrite the previous equation as

$$\tau \dot{A} = -A + S(\lambda(J \cdot A + \varepsilon I - \theta)),$$

and perform the change of variable $V = J \cdot A + \varepsilon I - \theta$. This leads to the following equations

$$\begin{cases} \tau \dot{V}(x, t) = -V(x, t) + \int_{-\pi/2}^{\pi/2} [J_0 + J_1 \cos(\alpha(y - x))] S(\lambda V(y, t)) dy / \pi + \varepsilon I(x) - \theta \\ I(x) = 1 - \beta + \beta \cos(\alpha(x - x_0)) \end{cases} \quad (5.2)$$

We are now in the case of the model studied in this paper with $p = 1$, $d = 1$ and $\Omega = (-\pi/2, \pi/2)$. Note that since the x -coordinate represents an angle, this is not a neural field model per se but rather a neural mass model.

The nonlinearity is often chosen to be a Heaviside function, or, as in [4], a piecewise linear approximation of the sigmoid ⁷, or, as in [20, 19, 10], a true sigmoidal function. J_1 can take any sign and I is an external current coming from the LGN. J_0 is most of the time negative (see [4, 19, 10, 12]) but can be positive as well (see [12]): the J_i s can be thought of as the first Fourier coefficients of J , J_0 , being its mean value. We can, up to a multiplication of the previous equation, make the assumption

$$J_0 = \varepsilon_0 \in \{-1, 1\}$$

For example, in [19], we find $J_0 = -7.3$, $J_1 = 11$, $\beta = 0.1$, $\theta = 0$ which are taken from [4] except for $\theta = 1$. The slope is assumed to be $\lambda = 1$. Using the previous scaling, it becomes $J_0 = -1$, $J_1 = 1.5$, $\lambda = 7.3/s_1 = 29.2$ and $\theta \rightarrow \theta/7.3$ which gives $\theta \approx 0.1$ in the case of [4] and $\theta = 0$ in [19].

The goal of this section is not to derive the whole bifurcation diagram of the Ring Model but rather to show how the stationary solutions are organized and to give clues about the dynamics in a given range of parameters. This study is helpful because many large scale model of V1 use the Ring Model for the hypercolumns. We will see that, depending on the stiffness of the nonlinearity, there may exist many stationary solutions, which are all acceptable responses of the network for a given input of the LGN. Thus these local orientation detectors may behave less trivially than they were initially made for. These cortical states can make the local dynamics sophisticated when the slope parameter λ is big enough.

5.1. Mapping the ring model to the PG-kernel formalism. Expanding the cosine in the previous equation, and denoting by \cos_α (respectively \sin_α) the function $x \rightarrow \cos(\alpha x)$ (respectively $x \rightarrow \sin(\alpha x)$), we find that, depending on the sign of J_i , ($\varepsilon_i = \text{sign}(J_i)$, $i = 0, 1$):

$$J = \varepsilon_0 1 \otimes 1 + \varepsilon_1 \sqrt{|J_1|} \cos_\alpha \otimes \sqrt{|J_1|} \cos_\alpha + \varepsilon_1 \sqrt{|J_1|} \sin_\alpha \otimes \sqrt{|J_1|} \sin_\alpha = \sum_{i=0}^2 \varepsilon_i X_i \otimes X_i, \\ \varepsilon_2 = \varepsilon_1.$$

⁷This does not allow the computation of bifurcation branches but allows the detection of branching points.

This formulation has the advantage of preserving the symmetries of \mathbf{W} . With the notations of the previous section, we have $I^\perp = 0$, and

$$\tau \dot{V}^\parallel = -V^\parallel + W \cdot S(\lambda(V^\parallel + V_0^\perp e^{-t/\tau})) + \varepsilon I^\parallel - \theta$$

where

$$V^\parallel(x, t) = v_1(t) + v_2(t)\sqrt{|J_1|}\cos_\alpha x + v_3(t)\sqrt{|J_1|}\sin_\alpha x, \quad (5.3)$$

i.e. the model is three-dimensional. Note that the previous equation is a rewriting of (5.2) **without any approximation**.

Similarly we have

$$I = I^\parallel = 1 - \beta + \frac{\beta \cos_\alpha x_0}{\sqrt{|J_1|}} \overbrace{\sqrt{|J_1|}\cos_\alpha x}^{X_1} + \frac{\beta \sin_\alpha x_0}{\sqrt{|J_1|}} \overbrace{\sqrt{|J_1|}\sin_\alpha x}^{X_2} \quad (5.4)$$

As $V^\perp(t) \rightarrow 0$, we restrict the study to the case $V^\perp = 0$ even if we lose some of the 'real' dynamics by doing so. This is motivated by the fact that the dynamics is made of heteroclinic orbits (as we will see in a moment) between persistent states belonging to the vector space $V^\perp = 0$. Hence, using this simplification, we are led to study the following 3D system:

$$\begin{cases} \tau \dot{v}_1 = -v_1 + \varepsilon_0 \langle S(\lambda V), 1 \rangle + \varepsilon I_1^\parallel - \theta \\ \tau \dot{v}_2 = -v_2 + \varepsilon_1 \sqrt{|J_1|} \langle S(\lambda V), \cos_\alpha \rangle + \varepsilon I_2^\parallel \\ \tau \dot{v}_3 = -v_3 + \varepsilon_1 \sqrt{|J_1|} \langle S(\lambda V), \sin_\alpha \rangle + \varepsilon I_3^\parallel \end{cases} \quad (5.5)$$

where $\langle f, g \rangle = \int_{-\pi/2}^{\pi/2} f(x)g(x) \frac{dx}{\pi}$, V is given by equation (5.3) and $I_i^\parallel, i = 1, 2, 3$ is given by equation (5.4). Note that the basis (X_0, X_1, X_2) is not orthogonal for this inner product.

This system enjoys the symmetries described by the following lemma.

LEMMA 5.1. *When $I_3^\parallel = 0$, if $\mathbf{v} = (v_1 \ v_2 \ v_3)$ is a solution, then so is $(v_1 \ v_2 \ -v_3)$. The plane $v_3 = 0$ is invariant by the dynamics.*

Proof. This is a consequence of the fact that \sin_α is an odd function while \cos_α is an even function. \square

It is easy to see that

$$E(\mathbf{v}) = -\frac{\langle \mathbf{v}, \Gamma \mathbf{v} \rangle}{2\tau} + \frac{1}{\tau\lambda} \int_{-\pi/2}^{\pi/2} \bar{S}_0(\lambda v_1 \varepsilon_0 + \lambda v_2 \varepsilon_1 \sqrt{|J_1|} \cos_\alpha x + \lambda v_3 \varepsilon_1 \sqrt{|J_1|} \sin_\alpha x) \frac{dx}{\pi} + \langle \varepsilon I^\parallel - \theta, \Gamma \mathbf{v} \rangle,$$

where \bar{S}_0 is a primitive of S_0 and $\Gamma = \text{diag}(\varepsilon_0, \varepsilon_1, \varepsilon_2)$, is an energy function for the dynamics, *i.e.* $\dot{\mathbf{v}} = \Gamma \cdot \nabla E(\mathbf{v})$. Consequently, even for I non spatially homogenous, there are no non-constant periodic trajectories nor homoclinic orbits⁸. Moreover, all bounded trajectories are stationary solutions or trajectories converging to stationary solutions. Having proven that

⁸This follows from the consideration of the time derivative of the energy E .

all trajectories are bounded for the neural field equations in proposition 2.6, we have characterized the dynamics. It remains to compute the stationary solutions and their attraction basins.

Remark 10. We can generalize these facts to PG-kernels of the type $\mathbf{J} = \sum_{i=0}^{N-1} \varepsilon_i X_i \otimes X_i$

by choosing $E(\mathbf{v}) = -\frac{\langle \mathbf{v}, \mathbf{L}\mathbf{v} \rangle}{2} + \frac{1}{\lambda} \sum_{k=1}^p \int_{\Omega} \bar{\mathbf{S}}(\sum_i \lambda \varepsilon_i v_i X_i^k(\mathbf{r})) d\mathbf{r} + \langle \mathbf{I}, \mathbf{v} \rangle$

5.2. Finding the persistent states. In order to characterize the set \mathcal{B} of stationary solutions, we apply the scheme of section 3.1. Hence we study the following equation

$$V = J \cdot S_0(\lambda V) + \varepsilon I^{\parallel} + \mu(-\theta + J \cdot S(0))$$

The nonlinearity is the *odd* function :

$$S_0(x) = \frac{1}{1 + e^{-x}} - \frac{1}{2}$$

Note that $J \cdot S(0) = \frac{1}{2}(\varepsilon_0 + J_1 \frac{2s \sin_{\alpha}(\pi/2)}{\alpha\pi} \cos_{\alpha}) = \frac{1}{2}\varepsilon_0 + \varepsilon_1 \sqrt{|J_1|} \frac{\sin_{\alpha}(\pi/2)}{\alpha\pi} X_1$. This gives :

$$\begin{cases} \tau \dot{v}_1 = -v_1 + \varepsilon_0 \langle S_0(\lambda V), 1 \rangle + \varepsilon I_1^{\parallel} + \mu(-\theta + \frac{\varepsilon_0}{2}) \\ \tau \dot{v}_2 = -v_2 + \varepsilon_1 \sqrt{|J_1|} \langle S_0(\lambda V), \cos_{\alpha} \rangle + \varepsilon I_2^{\parallel} + \mu \varepsilon_1 \sqrt{|J_1|} \frac{\sin_{\alpha}(\pi/2)}{\alpha\pi} \\ \tau \dot{v}_3 = -v_3 + \varepsilon_1 \sqrt{|J_1|} \langle S_0(\lambda V), \sin_{\alpha} \rangle + \varepsilon I_3^{\parallel} \end{cases} \quad (5.6)$$

5.2.1. The simpler case $\mu = \varepsilon = 0$. This corresponds to finding the persistent states when $\mu = \varepsilon = 0$ ensuring that $\mathbf{v} = 0$ is a solution. For the sake of simplicity, we reduce the study to the case $\alpha \neq 2$ which breaks the translation symmetry so that we do not get involved with equivariant bifurcation theory.

The Jacobian at $\mathbf{v} = 0$ is given by (using some symmetries):

$$-\text{Id}_{3 \times 3} + \lambda s_1 \mathbf{K},$$

where $s_1 = S_0^{(1)}(0) = \frac{1}{4}$ and the matrix \mathbf{K} is equal to

$$\mathbf{K} = \begin{bmatrix} \varepsilon_0 & \varepsilon_0 \sqrt{|J_1|} \langle 1, \cos_{\alpha} \rangle & 0 \\ \varepsilon_1 \sqrt{|J_1|} \langle 1, \cos_{\alpha} \rangle & J_1 \langle 1, \cos_{\alpha}^2 \rangle & 0 \\ 0 & 0 & J_1 \langle 1, \sin_{\alpha}^2 \rangle \end{bmatrix}$$

\mathbf{K} has in general (for $\alpha \approx 2$) three real eigenvalues. Indeed the operator J is self-adjoint for the inner-product defined above, but, as previously mentioned, the basis (X_0, X_1, X_2) is not orthogonal for this inner product, and hence the matrix \mathbf{K} is not symmetric in this basis. We note σ_1 the eigenvalue of \mathbf{K} corresponding to the eigenvector $(0, 0, 1)$, σ_2 and σ_3 the two eigenvalues of its upper left-hand 2×2 submatrix. The values, noted λ_i , $i = 1, 2, 3$, corresponding to potential⁹ bifurcations are equal to $4/\sigma_i$. The signs of the λ_i s give the number of bifurcated branches (recall that $\lambda > 0$). Because $s_2 = S_0^{(2)}(0) = 0$ and $s_3 = S_0^{(3)}(0) = -1/8 \neq 0$, all branches are Pitchfork branches (see section.3.1) whose third order term is $\chi_3^{(i)} = \lambda_i^2 \frac{s_3}{6s_1} \langle e_i^3, e_i^* \rangle_2 (\approx \lambda_i^2 \frac{s_3}{6s_1} \|e_i^2\|_2^2 < 0$ for $\alpha \approx 2$). Hence these branches are directed toward $\lambda > \lambda_i$. This is summarized in table 5.1: The eigenvectors e_i , $i = 1, 2, 3$, of

⁹The upcoming nonlinear analysis will show that they are indeed bifurcation points.

	ε_1	-1	1
ε_0			
-1		0	2
1		1	3

TABLE 5.1

Number of bifurcated Pitchfork branches from $(0, \lambda)$ depending on the values of $\varepsilon_0, \varepsilon_1$. The value of α in (5.2) is close to 2.

the Jacobian of (5.5) at $\mathbf{v} = 0$ are given by:

$$e_1 = \sin_\alpha, \quad e_{2,3} = a_{2,3} + b_{2,3} \cos_\alpha$$

We reduce the number of possibilities by assuming from now on that $J_1 > 0$. It turns out that in this case $\sigma_2 < 0$ and there are only two possibilities to consider: $\sigma_1 < \sigma_3$ for $\alpha > 2$ and $\sigma_3 < \sigma_1$ for $\alpha < 2$. This gives the relative position of the different bifurcated branches, noted $P_i, i = 1, 3$. Once we have found the bifurcation point, we can numerically compute the bifurcated branches for all positive values of λ using a continuation method (we used the pseudo-arc length method as described for example in [48, 38]).

From our numerical experiments we conjecture that in the case $\varepsilon_0 = -1$ and $\varepsilon_1 = 1$, P_1 and P_3 satisfy the following properties

1. P_1 lies on the v_3 -axis.
2. P_3 lies in the plane of equation $v_3 = 0$.
3. P_1 and P_3 do not intersect.

Remark 11. We can reverse the orientation of the pitchforks by choosing a nonlinearity such that $s_3 > 0$, the bifurcation diagram would be more complex: more saddle node points would appear because of proposition 3.3. It is the fact that $s_2 = 0$ for the sigmoid which produces pitchfork branches. Another choice of nonlinearity, for example $S(x) = \frac{1}{1+\exp(-x+\varepsilon)}$, would produce transcritical branches. It is indeed difficult to imagine that $s_2 = 0$ for an experimental fit of a “real” rate function. But anyway we are not yet looking at the “real” bifurcation diagram since we are assuming $\varepsilon = \mu = 0$.

Figure 5.1 shows a typical example corresponding to the values of the parameters that are found in the largest number of published articles. We come back to this choice in section 5.3. The left part of the figure shows the three components of the persistent states as functions of λ . For P_1 there is only one non-zero component, v_3 , in blue. For P_3 there are two non-zero components, v_1 shown in red and v_2 shown in green. The right part of the figure shows another representation of P_1 and P_3 as curves parametrized by λ in the (v_1, v_2, v_3) space. P_3 is clearly in the (v_1, v_2) plane while P_1 is along the v_3 -axis. The color at each point of the curves represents the value of λ according to the color scale shown on the right.

In detail we have

$\lambda_3 < \lambda < \lambda_1$ When λ goes through λ_3 , the 0-solution loses its stability and becomes a saddle. There are three persistent states, 0 (unstable node) and two located on the pitchfork branch P_3 , both stable. The corresponding dynamics is shown in the left part of figure 5.1.

$\lambda_1 < \lambda$ When λ goes through λ_1 , the 0-solution loses its stability along the v_3 -axis. There are two new persistent states located on the pitchfork branch P_1 , both are unstable nodes (the unstable manifold is one-dimensional). The corresponding dynamics is also shown in the left part of figure 5.1.

There are at most 5 stationary solutions.

Remark 12. In the case $J_0 = 1$ and $\varepsilon_1 = 1$, there is another pitchfork branch to handle,

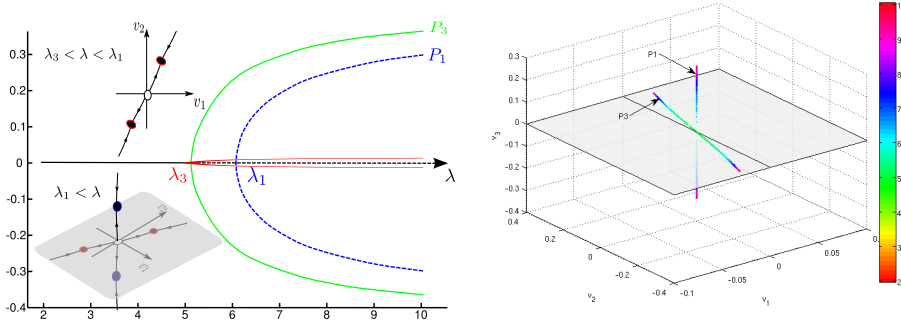


FIG. 5.1. Left: Plot of the bifurcation diagram for $\alpha = 2.2$. It shows the two pitchfork branches P_1 and P_3 . For each branch, we have only plotted the non-zero coordinates with $v_1 = \text{red}$, $v_2 = \text{green}$ for P_3 and $v_3 = \text{blue}$ for P_1 . We have also plotted the dynamics in two and three dimensions according to the values of the slope parameter λ . Right: Plot of the equilibrium points. The color encodes the value of the slope λ (see text). $J_0 = -1$, $J_1 = 1.5$, $\mu = 0$, $\varepsilon = 0$, $\alpha = 2.2$

see table 5.1. For λ big enough, $\mathbf{v} = 0$ becomes an unstable node and there are 7 stationary solutions instead of 5 in the case $J_0 = -1$

5.2.2. The case $\mu = 1$, $\varepsilon \neq 0$. We are now halfway from our scheme completion. To have an idea of the persistent states at low contrast (*i.e.* $\varepsilon \approx 0$), we need to know the persistent states for : $\lambda, \mu = 1, \varepsilon = 0$, that is we need to know the solutions of

$$V_\lambda^f = J \cdot S(\lambda V_\lambda^f) - \theta$$

Following our program, we numerically compute the persistent states when the slope λ and μ both vary. As described in section 2.3 we expect many of the previous bifurcations to disappear thereby breaking some of the connectivity of the sets \mathcal{B}_λ which can actually be (partially) recovered by considering the sets $\mathcal{B}_{\lambda, \mu}$. This was done using the library TRILINOS (see [48] and the website) using multiparameters continuation.

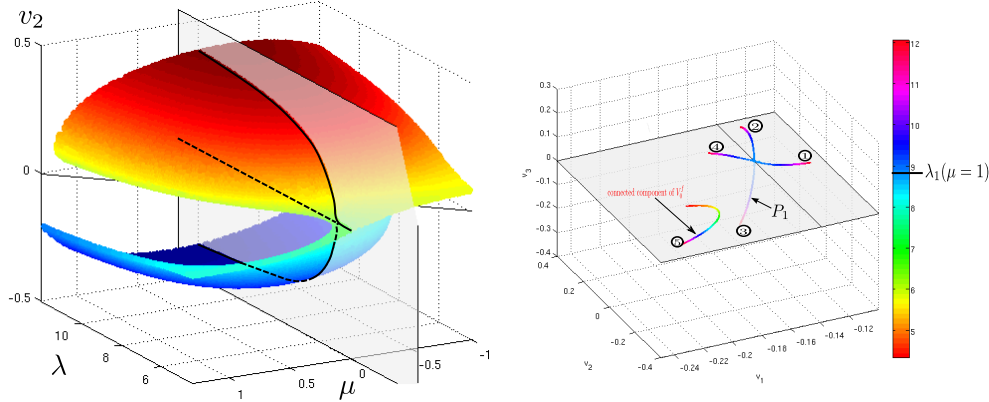


FIG. 5.2. Left: The v_2 component of the 2-parameters continuation (λ, μ) for $\theta = 0.1$, $\alpha = 2.2$, $J_0 = -1$, $J_1 = 1.5$. Right: Plot of the equilibrium points. The color encodes the value of the slope λ . $J_0 = -1$, $J_1 = 1.5$, $\mu = 1$, $\varepsilon = 0$, $\alpha = 2.2$, $\theta = 0.1$.

We show an example of this continuation in figure 5.2.Left where we display the v_2 component of the persistent states as a function (sometimes multivalued) of λ and μ . A cross-

section of this set by the plane of equation $\mu = 0$ (shown as semi-transparent in the figure) yields a curve identical to the one shown in green figure 5.1.Left. The figure nicely shows how the first pitchfork bifurcation branch P_3 opens up when μ becomes non zero: this gives the connected component of \mathbf{V}_λ^f which is linearly stable.

$$\begin{cases} 0 = v_1 - \varepsilon_0 \langle S_0(\lambda V), 1 \rangle + \mu(-\theta + \frac{\varepsilon_0}{2}) \\ 0 = v_2 - \varepsilon_1 \sqrt{|J_1|} \langle S_0(\lambda V), \cos_\alpha \rangle + \mu \varepsilon_1 \sqrt{|J_1|} \frac{\sin_\alpha(\pi/2)}{\alpha\pi} \\ 0 = v_3 - \varepsilon_1 \sqrt{|J_1|} \langle S_0(\lambda V), \sin_\alpha \rangle \end{cases} \quad (5.7)$$

However, as can be seen from 5.2.Right, non-zero values of μ do not break the pitchfork P_1 . It is easy to qualitatively understand why, even though a full mathematical proof is hard to come up with: μ does not affect the third equation which produces the pitchfork P_1 . We can prove it locally for μ near 0 using the implicit function theorem. We are looking for a point $(v_1(\mu), v_2(\mu), 0)$ at which a pitchfork occurs for $\lambda = \lambda_1(\mu)$. Let us consider

$$H(v_1, v_2, \lambda; \mu) = \begin{bmatrix} v_1 - \varepsilon_0 \langle S_0(\lambda V), 1 \rangle + \mu(-\theta + \frac{\varepsilon_0}{2}) \\ v_2 - \varepsilon_1 \sqrt{|J_1|} \langle S_0(\lambda V), \cos_\alpha \rangle + \mu \varepsilon_1 \sqrt{|J_1|} \frac{\sin_\alpha(\pi/2)}{\alpha\pi} \\ 1 - \lambda J_1 \langle DS_0(\lambda v_1 X_0 + \lambda v_2 X_1), \sin_\alpha^2 \rangle \end{bmatrix} \quad (5.8)$$

where the last component of $H(v_1, v_2, \lambda; \mu)$ is the partial derivative with respect to v_3 of the third equation in (5.7). It is easy to see that $H(0, 0, \lambda_1; 0) = [0 \ 0 \ 0]$. The Jacobian of H w.r.t. (v_1, v_2, λ) at $(0, 0, \lambda_1, 0)$ is (because $S^{(2)}(0) = 0$):

$$\begin{bmatrix} -1 + \lambda_1 s_1 \varepsilon_0 & \lambda_1 s_1 \varepsilon_1 \sqrt{|J_1|} \langle 1, \cos_\alpha \rangle & 0 \\ \lambda_1 s_1 \varepsilon_0 \sqrt{|J_1|} \langle 1, \cos_\alpha \rangle & -1 + \lambda_1 s_1 J_1 \langle 1, \cos_\alpha^2 \rangle & 0 \\ 0 & 0 & -s_1 J_1 \langle 1, \sin_\alpha^2 \rangle \end{bmatrix} \in GL_3(\mathbb{R})$$

Hence there exists a unique solution defined locally for $\mu \geq 0$ satisfying $H(v_1(\mu), v_2(\mu), \lambda_1(\mu); \mu) = 0$: we have found a bifurcated point. Moreover, as $\chi_1^{(3)}(\mu = 0) \neq 0$, it will remains so for small μ : the Pitchfork P_1 is not affected by μ . For large values of μ we have to rely on numerical simulations.

Now, because of lemma 5.1, the solutions (v_1, v_2) corresponding to $v_3 \neq 0$ (*i.e.* lying on the pitchfork branch) are the same for v_3 and $-v_3$ which gives the branch 2-3 in figure 5.3. Hence, when $\mu \neq 0$, we still have the pitchfork P_1 and the branch (located in $v_3 = 0$) arising from the opening of P_3 . This gives the diagram shown in figure 5.3 for the three components of \mathbf{v} . The left part of the figure shows the case $\mu = 0.2$ while the right part shows the case $\mu = 1$, the one we are interested in. Each triplet of (red,green,blue) curves represents the variation of (v_1, v_2, v_3) as a function of the parameter λ . They are labeled by integers between 1 and 5.

This diagram is a bit misleading because if we count the *red* components, there are four of them for $\lambda > \lambda_1$ which gives an even number of solutions (in contradiction with proposition 2.9). In fact by doing so we miss the symmetry $v_3 \leftrightarrow -v_3$ and the corresponding solutions. It is easier to look at figure 5.2.Right to count the stationary solutions.

From section 3.1, it follows that the connected branch of V_0^f is stable as well as the branch P_1 . The only unstable branch comes from the opening of P_3 and is shown in figure 5.2.Right.

Remark 13. Figure 5.2 gives a good example where our scheme allows to detect another branch of solutions which is not connected to the connected component of the trivial solution. Figure 5.3 also tells us which branches will appear when the contrast satisfies $\varepsilon \neq 0$: this will

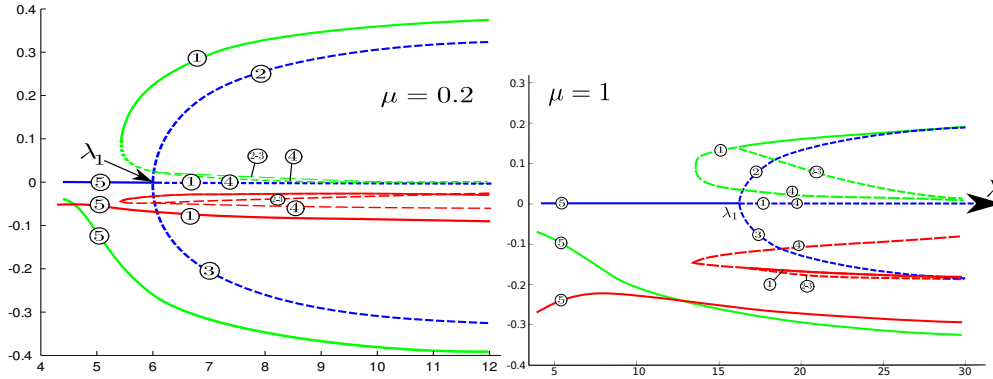


FIG. 5.3. Plot of the three components $(v_1, v_2, v_3) = (\text{red, green, blue})$ as functions of the slope λ for the following values of the parameters: $J_0 = -1$, $J_1 = 1.5$, $\mu = 1$, $\varepsilon = 0$, $\alpha = 2.2$, $\theta = 0.1$. Remember that the slope of the model has to be around $\lambda = 29$ in order to be compatible with previous work.

be a perturbation of figure 5.2. Except in the case $x_0 = 0$ (see equation (5.2)), the pitchfork P_1 will open up, giving two other connected components in addition to the connected component of \mathbf{V}_0^f .

To illustrate further these ideas we have plotted in figures 5.4, 5.5 and 5.6 all the persistent states (i.e. the functions $A^f(x) = S(V^f(x))$ for $-90^\circ \leq x \leq 90^\circ$) for various values of the slope λ , and the contrast ε . In detail we have $\varepsilon I(x) = \varepsilon(1 - 0.1 + 0.1 \cos_\alpha(x - 0.1))$, $\alpha = 2.2$, $J_0 = -1$, $J_1 = 1.5$, and $\mu = 1$. Unstable solutions are shown in dotted lines, stable solutions in continuous lines. The width of the continuous lines is proportional to the smallest magnitude of the (negative) eigenvalues of the Jacobian of the system for this solution. We show in appendix F that this magnitude is a lower bound of the size of the corresponding attraction basin. The external current $I(x)$ is plotted as a red continuous line in figures 5.5 and 5.6.

Figures 5.4 and 5.5 correspond to the cases $\varepsilon = 0$ (no input current) and $\varepsilon = 0.05$, respectively. In each figure the three subfigures correspond, from left to right, to the increasing values 14, 20, and 29 of the slope λ . In the case of figure 5.4 the number and the stability of the solutions can be predicted directly from the righthand side of figure 5.3 while for figure 5.5 this can be achieved from a perturbation of the same figure. Note that, except for the unstable solution peaking at $x = 0^\circ$, the effect of increasing the slope of the sigmoid is to increase the amplitude of the solutions, as can be seen from an examination of the branches labelled 4 in the righthand side of figure 5.3.

Figure 5.6 corresponds to an even higher current than in figure 5.5, i.e. the contrast ε is equal to 0.1. In this case we only show the stationary solutions for the values 20 and 29 of the slope parameter because there is little difference between the cases $\lambda = 14$ and $\lambda = 20$. We note that the effect of increasing the slope is the same as in figure 5.5 and that for a given slope, the effect of increasing the contrast ε is also to increase the amplitude of the solutions, except for the unstable solution peaking at $x = 0^\circ$. The labels of the five solutions are the same as in figure 5.3. The reader should have no problem to transfer them to the solutions plotted in figures 5.4 and 5.5.

5.3. Discussion. There are two reasons why we presented this example. First, it is a nice simple model to which the formalism of this article easily applies and allows us to push the analysis far enough to grasp an almost complete understanding of its persistent states and a somewhat detailed understanding of its dynamics. Second, it conveys information for

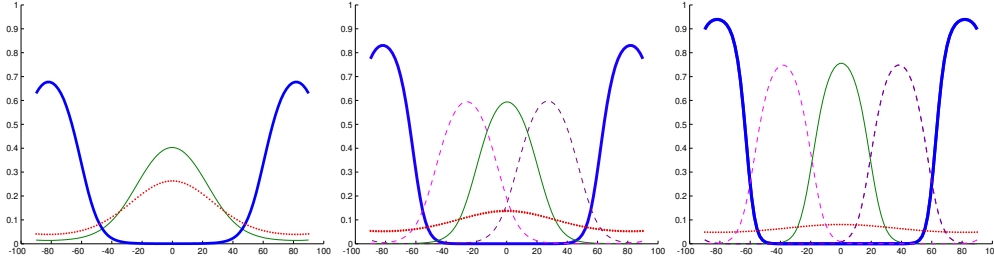


FIG. 5.4. Stationary solutions for the ring model with no input current ($\varepsilon = 0.0$) for three values of the slope parameter λ . From left to right $\lambda = 14, 20, 29$. For $\lambda = 14$ there are three solutions, two stable (shown in continuous line) and one unstable (shown in dotted lines). For $\lambda = 20$ and $\lambda = 29$ there are five solutions, two stable, and three unstable, see text.

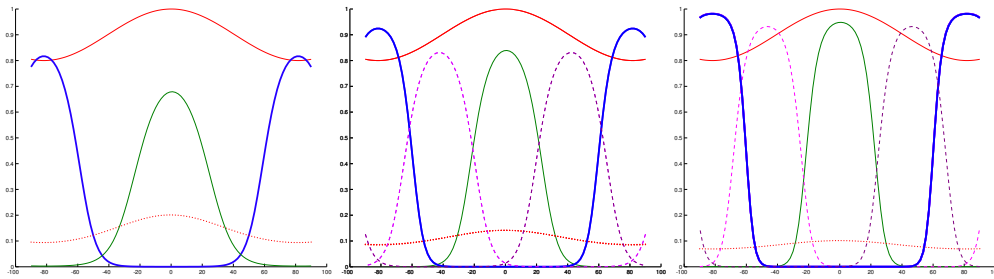


FIG. 5.5. Stationary solutions for the ring model with an input current corresponding to the contrast $\varepsilon = 0.05$ for three values of the slope parameter λ . From left to right $\lambda = 14, 20, 29$. In all the cases there are at most five solutions, two of them stable (shown in continuous lines), and three (one for $\lambda = 14$) unstable (shown in dotted lines), see text.

models of V1 that is likely to be biologically relevant. For example, as the slope λ of the sigmoid is increased, many (up to 4 depending on the signs of (J_0, J_1)) new stationary states appear whose stability evolves with λ . One of these solutions is “dramatic” for the purpose of orientation detection: even if the LGN input orientation peaks around the angle $x_0 = 0$, the Ring Model can produce a stable cortical state (or a percept) corresponding to an angle of $\pi/2$!

However these solutions may be destabilized by adding lateral spatial connections in a spatially organized network of ring models; it remains an area of future investigation. As far as we know, only Bressloff and co-workers looked at this problem (see [11, 12]): they studied the local dynamics around the bifurcation points but did not look at non-local dynamics (basically they considered that there were 2 stationary solutions around a bifurcation point and forgot about the third one predicted by proposition 2.9).

There is no biologically motivated restriction on the values of the slope λ which can be as large as desired, without mentioning the fact that neural mass models are very often written with a Heaviside function for the nonlinearity which, as mentioned previously, is the limit case: $H(x) = \lim_{\lambda \rightarrow \infty} S(\lambda x)$.

We also made the assumption $\alpha \neq 2$ in the previous analysis. It remains to know how much of the preceding holds in the case $\alpha = 2$. More generally, what would remain if one were to choose a difference of Gaussians as a connectivity function over a cortex $\Omega = (-\pi/2, \pi/2)$. We expect a lot of similarities if the width of the difference of Gaussians is of the same order of $\cos \alpha$.

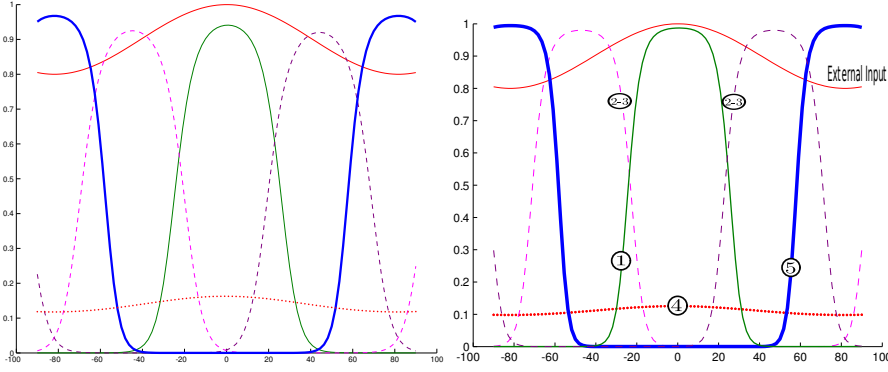


FIG. 5.6. Stationary solutions for the ring model with an input current corresponding to the contrast $\varepsilon = 0.1$ for two values of the slope parameter λ . From left to right $\lambda = 20, 29$. In both cases there are five solutions, two of them stable (shown in continuous lines), and three unstable (shown in dotted lines), see text.

6. Two populations of spatially organized neurons. We now apply the previous analysis to a system we started to analyse in [26]. In the somewhat reduced form we consider here, it consists of two populations ($p = 2$), one excitatory, one inhibitory, distributed over a flat ($d = 2$) cortex $\Omega = [-1, 1]^2$. The connectivity matrix kernel writes:

$$\mathbf{J}(\mathbf{r}, \mathbf{r}') = \begin{bmatrix} aG_{11}(\mathbf{r} - \mathbf{r}') & -bG_{12}(\mathbf{r} - \mathbf{r}') \\ bG_{21}(\mathbf{r} - \mathbf{r}') & -cG_{22}(\mathbf{r} - \mathbf{r}') \end{bmatrix} \quad (6.1)$$

where the $G_{ij}(\mathbf{r}) = e^{-\frac{\|\mathbf{r}\|^2}{2\sigma_{ij}^2}}$ are two-dimensional Gaussian functions defined on \mathbb{R}^2 with $G_{12} = G_{21}$. $a, b, c > 0$ characterize the strength of the connections. We also assume $\mathbf{I}_{ext} = 0$. The parameter μ controlling the translation of the sigmoid (see (3.3)) is therefore the only parameter, outside λ , that we will vary from 0 to 1. We also chose (notice that $s_2 \neq 0$):

$$S(x) = \frac{1}{1 + e^{-x+\theta}}, \quad \theta = 1.3$$

In [26], we were able to compute the stationary solutions $\mathbf{V}_{\lambda, \mu=1}^f$ when the slope λ was small (*i.e.* $\lambda < \lambda^*$) using the Nystrom method. We now know that if we perform a continuation of these solutions with respect to λ , we are bound to miss quite a few of them. Therefore we perform a two-parameter continuation with respect to the pair (λ, μ) in order to recover more, if not all, stationary solutions.

Biologically speaking, no systematic investigation has been performed to test the validity of the translation invariance of the connectivity function. Hence a roughly translation invariant (called heterogeneous in [21]) is not less biologically relevant. This is where the PG-kernels are useful: they provide an easy way to approximate the convolution operation as well as an effective representation of the connectivity (see section 4).

There are four reasons why we think this example is interesting:

- We want to show how to deal with heterogeneous kernels.
- We want to give a non trivial example to the existence of a branch of solutions not connected to the trivial solution \mathbf{V}_0^f .
- We want to show an example of application of proposition 3.3.
- More importantly, we want to show how the results of section 3.1.1 may change in the two-dimensional case.

As in the previous case, we are not interested in having the complete bifurcation diagram of the system but rather in giving numerical examples of the previously enumerated points.

6.1. PG-kernel approximation of \mathbf{J} . Let us write

$$e^{-\|\mathbf{r}-\mathbf{r}'\|^2/2} = e^{-\|\mathbf{r}\|^2/2} e^{-\|\mathbf{r}'\|^2/2} e^{\langle \mathbf{r}, \mathbf{r}' \rangle} \approx e^{-\|\mathbf{r}\|^2/2} e^{-\|\mathbf{r}'\|^2/2} \left(1 + \langle \mathbf{r}, \mathbf{r}' \rangle + \frac{1}{2} \langle \mathbf{r}, \mathbf{r}' \rangle^2 + \dots \right)$$

We notice two important facts:

- $1 + \langle \mathbf{r}, \mathbf{r}' \rangle + \frac{1}{2} \langle \mathbf{r}, \mathbf{r}' \rangle^2 + \dots$ is a polynomial in the components of \mathbf{r} and \mathbf{r}' , hence a PG-kernel.
- $e^{-\|\mathbf{r}\|^2/2}$ has a bell-shape which we approximate with the following function $\left(1 - \|\mathbf{r}\|^2\right)^a$ with $a > 0$. This choice is also motivated by the fact that $e^{-\|\mathbf{r}\|^2/2}$ tends to zero at the edges of the infinite cortex that is usually considered in the literature. We keep this property with our finite cortex since $\left(1 - \|\mathbf{r}\|^2\right)^a = 0$ on the boundary $\partial([-1, 1]^2)$ of $[-1, 1]^2$. Any other positive bell shaped function would be appropriate.

Putting these two facts together, we end-up with the following approximation of a Gaussian convolution kernel with a PG-kernel.

$$J_{ij}(\mathbf{r}, \mathbf{r}') = C_{ij} + \left(1 - \|\mathbf{r}\|^2\right)^{a_{ij}} \left(1 - \|\mathbf{r}'\|^2\right)^{a'_{ij}} P_{ij}(\mathbf{r}, \mathbf{r}'), \quad i, j = 1, 2 \quad (6.2)$$

where \mathbf{P} is a 2×2 matrix with polynomial entries in \mathbf{r} and \mathbf{r}' and \mathbf{C} is a constant 2×2 matrix.

Remember from section 2.1 that for $d = 2$, we require $m = 1$, i.e. $\mathcal{F} = \mathbf{W}^{1,2}(\Omega, \mathbb{R}^2)$. Thus $\|\mathbf{J}\|_{\mathcal{F}} < \infty$ imposes $2(a_{ij} - 1) > -1$ hence $a_{ij} > 1/2$, similarly for a'_{ij} .

6.2. Numerical experiments. In these numerical experiment we choose $a_{11} = a'_{11} = 3$, $a_{12} = a'_{12} = a_{21} = a'_{21} = 2$, $a_{22} = a'_{22} = 4$, $a = 10$, $b = 15$, $c = 12.75$ and $\mathbf{L} = 0.5Id$. The polynomials $P_{ij}(\mathbf{r}, \mathbf{r}')$ are equal to the 4th-order Taylor expansion of $e^{\frac{\langle \mathbf{r}, \mathbf{r}' \rangle}{\sigma_{ij}}}$, with $\sigma_{ij}^{-1} = a_{ij}$.

This results in the following expressions for the two components V_1^f and V_2^f of the persistent state \mathbf{V}^f :

$$\begin{aligned} V_1^f &= Q_{11}(\mathbf{r}) \left(1 - \|\mathbf{r}\|^2\right)^3 + Q_{12}(\mathbf{r}) \left(1 - \|\mathbf{r}\|^2\right)^2 \\ V_2^f &= Q_{21}(\mathbf{r}) \left(1 - \|\mathbf{r}\|^2\right)^2 + Q_{22}(\mathbf{r}) \left(1 - \|\mathbf{r}\|^2\right)^4 \end{aligned}$$

The polynomials Q_{ij} , $i, j = 1, 2$ are of degree 4. The total number of parameters needed for representing a persistent state is therefore equal to $5 \times 5 \times 4 = 100$ variables. This number comes from the fact that we have four polynomials Q_{ij} , $i, j = 1, 2$, of total degree 10 in two variables that are the products of two polynomials in one variable of degree 4. The reason for this is the special form of the polynomials $P_{ij}(\mathbf{r}, \mathbf{r}')$ which are functions of the inner product $\langle \mathbf{r}, \mathbf{r}' \rangle$. This is a somewhat crude approximation of the convolution kernel (6.1).

Each of these 100 variables is a function of the slope parameter λ and contrast parameter μ . We represent in figure 6.1 the infinity norm of the 100-dimensional vector \mathbf{V}^f as a function of the slope parameter λ for $\mu = 0$.

All our analytical predictions are performed, for convenience and simplicity, on the convolution kernel \mathbf{J} . They are likely to carry over to the heterogeneous approximate case.

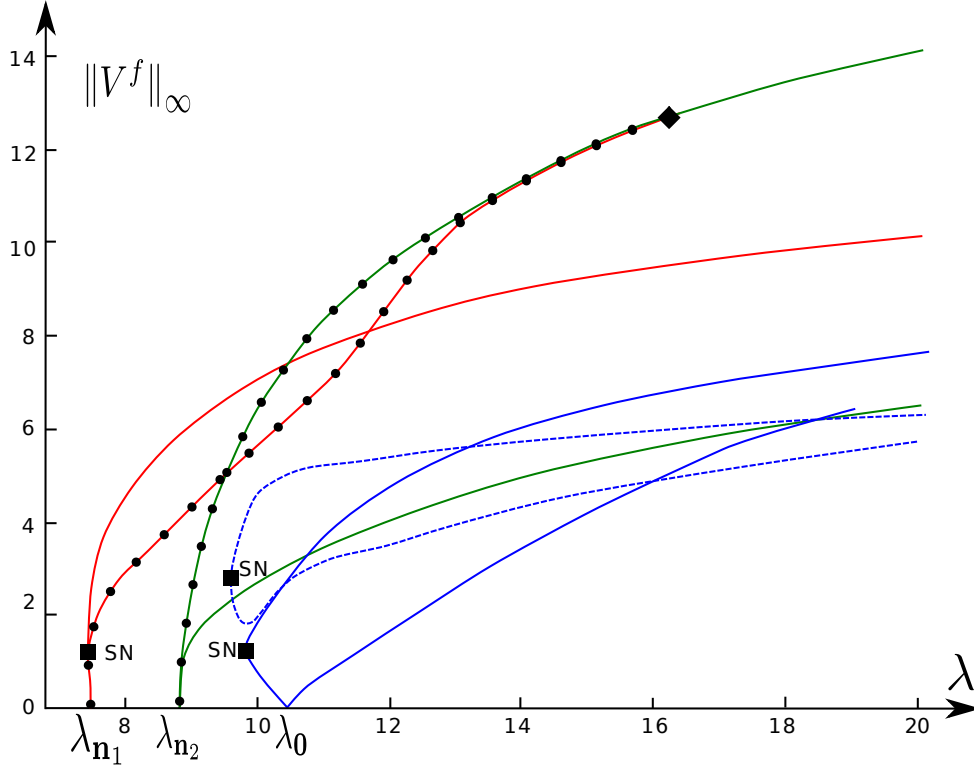


FIG. 6.1. Plot of the infinity norm $\|\cdot\|_\infty$ of the 100-dimensional vector \mathbf{V}^f as a function of the slope parameter λ for $\mu = 0$. Notice that $\mathbf{V}^f = 0$ is solution for all values of λ . The red and green branches corresponding to the values λ_{n_1} and λ_{n_2} of the slope parameter are marked with black disks and intersect at the point indicated by a black diamond. The dashed-line (blue) is a set of solutions that is not connected to the component corresponding to the trivial solution $\mathbf{V}^f = 0$. SN stands for saddle-node.

The general analysis having been conducted (see section 3.1), we wish to do some specific computations to explain the numerical results : the first thing to do is to find the eigen-elements of \mathbf{J} .

For each $\mathbf{n} = (n_1, n_2) \in \mathbb{N}$ consider the function $\cos_{\mathbf{n}} : \mathbb{R}^2 \rightarrow \mathbb{R}$ defined by $\cos_{\mathbf{n}}(\mathbf{r}) = \cos(n_1 r_1 + n_2 r_2)$, and the vector subspace $X_{\cos_{\mathbf{n}}}$ of \mathcal{F} defined by $X_{\cos_{\mathbf{n}}} = \{\mathbf{V} \mid \mathbf{V} = \cos_{\mathbf{n}} \mathbf{v}, \mathbf{v} \in \mathbb{R}^2\}$. $X_{\sin_{\mathbf{n}}}$ is defined in a similar fashion.

It is easy to check that the vector subspaces $X_{\cos_{\mathbf{n}}}$ of \mathcal{F} are invariant by the linear operator \mathbf{J} , and, by parity, that $\mathbf{J} \cdot X_{\sin_{\mathbf{n}}} = 0$ for all $\mathbf{n} \in \mathbb{N}^2$. We have

$$\mathbf{J} \cdot (\cos_{\mathbf{n}} \mathbf{v}) = \cos_{\mathbf{n}} \hat{\mathbf{J}}(\mathbf{n}) \mathbf{v} = \cos_{\mathbf{n}} \begin{bmatrix} a\hat{G}_1(\mathbf{n}) & -b\hat{G}_2(\mathbf{n}) \\ b\hat{G}_2(\mathbf{n}) & -c\hat{G}_3(\mathbf{n}) \end{bmatrix} \mathbf{v} \quad \forall \mathbf{v} \in \mathbb{R}^2$$

where $\hat{\mathbf{J}}, \hat{G}_i$ are the Fourier transforms of \mathbf{J} and G_i .

Keeping the notations of section 3.1, we find that

$$\sigma_{\mathbf{n}} \in \bigcup_{\mathbf{m} \in \mathbb{N}^2} \sigma(\hat{\mathbf{J}}(\mathbf{m}))$$

and the corresponding eigenvectors¹⁰ are in $X_{\cos_{\mathbf{n}}}$ for some $\mathbf{n} \in \mathbb{N}^2$, hence of the form $\cos_{\mathbf{n}} \mathbf{v}$

¹⁰We do not prove that we obtain all of them though it appears that these particular eigen-elements are sufficient

for some $\mathbf{v} \in \mathbb{R}^2$. We have chosen the Gaussians G_i such that the first eigenvalues are simple, hence each point $\lambda_{\mathbf{n}}$ is a bifurcation point: the corresponding *chi*-factors are

$$\chi_2^{(\mathbf{n})} \propto \langle \cos_{\mathbf{n}}^2, \cos_{\mathbf{n}} \rangle = 0 \text{ if } \mathbf{n} \neq \vec{0}$$

$$\chi_2^{(0)} \neq 0$$

Hence λ_0 is a transcritical bifurcation point whereas the other points $\lambda_{\mathbf{n}}$ are pitchfork bifurcation points. Depending on the vector \mathbf{v} , the orientation of the pitchfork may change.

In figure 6.1 (case $\mu = 0$), we see two pitchforks at $\lambda_{\mathbf{n}_1}$, $\lambda_{\mathbf{n}_2}$ and the transcritical branch at λ_0 . The first pitchfork at $\lambda_{\mathbf{n}_1}$ (red branch) is oriented toward the decreasing λ s, thus according to proposition 3.3, a saddle-node (noted SN in the figure) must appear. The same is true for the transcritical branch (continuous blue branch). Locally (near λ_0), each coordinate V_i^f , $i = 1, 2$ is 'flat', *i.e.* it looks like \cos_0 .

The bifurcation points $\lambda_{\mathbf{n}_1}$ and $\lambda_{\mathbf{n}_2}$ are connected by the red-dotted branch. It cannot be seen from this graph that this is true (because two states with the same norm may be different), but it can be checked by looking at the 100 components. We plot in figure 6.2 the stationary membrane potential V_1^f of the first population for different values of λ along the branch connecting $\lambda_{\mathbf{n}_1}$ to $\lambda_{\mathbf{n}_2}$.

The last interesting fact is that our multi-parameter scheme allows to compute branches that are not connected to the trivial solution (here $\mathbf{V}^f = 0$) as one can see in figure 6.1: the dashed blue branch cannot be detected by λ -continuation of the trivial solution $\mathbf{V}^f = 0$ because it does not intersect any branch coming from $\mathbf{V}^f = 0$. This, again, cannot be read directly from figure 6.2: one has to look at all 100 components.

Remark 14. We have chosen the parameters a, b, c such that the first three eigenvalues have zero imaginary parts. Numerically, most of the other eigenvalues $\sigma_{\mathbf{n}}$ have non-zero imaginary part leading to Hopf bifurcations. Other stationary bifurcation may appear for large slope values (*i.e.* $\lambda > 40$).

7. Discussion. In this section we briefly discuss two important aspects of our model with respect to the biology.

7.1. Is the cortex really finite?. An important aspect of our work is that we assume that the domain Ω is bounded, in agreement with the fact that biological systems have finite sizes. As pointed out in the introduction this has the effect of simplifying somewhat the functional analysis of the problem. Our analysis then relies essentially on the fact that the operator defined by the connectivity function is compact, hence also its Frechet derivative. The spectrum of this derivative is therefore at most countable, 0 being an accumulation point in the case it is infinite. The inverses of its positive eigenvalues (multiplied by 4, see equation (3.7)) determine the possible points of bifurcation of the steady-state solution with respect to the slope parameter λ . They accumulate at $+\infty$ but will in general have values smaller than the range of values biologically relevant. Assuming in the worst case that each of these values corresponds to a bifurcation, if they are very close to each other the task of the numerical continuation program will become extremely difficult. This situation occurs when the spread of the connectivity function \mathbf{J} is very small with respect to the size of the domain Ω , making the finite size assumption questionable from the practical viewpoint. In order to get a feeling for the domain of applicability of our theory we have done the following experiment. Assume

to explain the numerically observed facts.

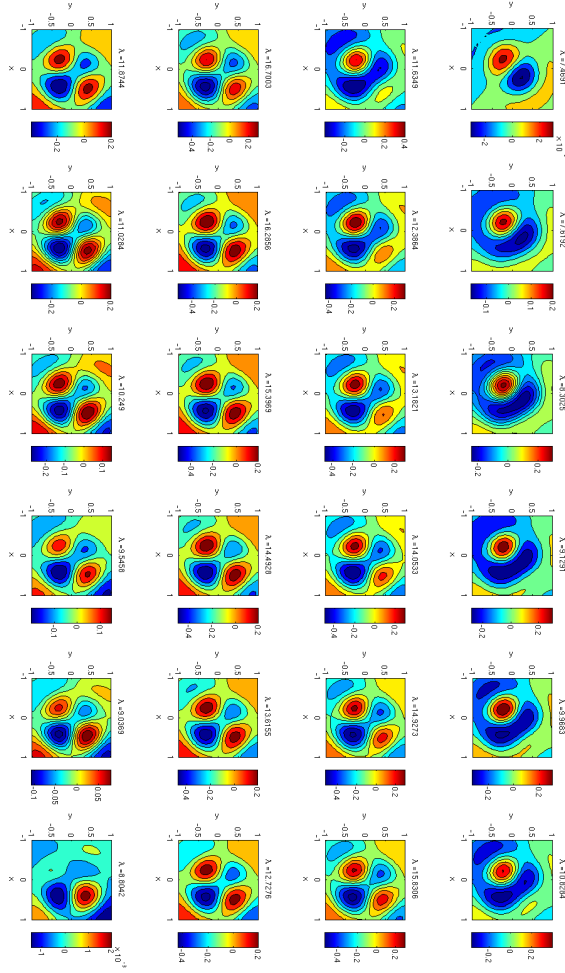


FIG. 6.2. Plot of the first component V_1^f of the solution \mathbf{V}^f along the red-green dotted branch connecting λ_{n_1} to λ_{n_2} in figure 6.1.

that the domain Ω is 1D, and of length a . Assume further that the local interaction is described by a Gaussian with zero mean and variance σ^2 normalized in such a way that its integral on the interval $[-a/2, a/2]$ is equal to 1. The eigenvalues σ_n of \mathbf{J} can be computed analytically as the Fourier coefficients of the function \mathbf{J} . As was just mentioned they accumulate at 0 since \mathbf{J} is compact. What is important is the separation of their inverses (the λ_n s). For a ratio σ/a equal to 10% the first 10 positive λ_n s are given by

n	1	2	3	4	5
	1.000	1.218	2.202	5.909	23.530
n	6	7	8	9	10
	139	1220	15785	337734	0.262989310 ⁷

If we decrease the ratio to 5% these numbers become

n	1	2	3	4	5
	1.000	1.051	1.218	1.559	2.202
n	6	7	8	9	10
	3.4341	5.909	11.224	23.530	54.445

and if we decrease the ratio to 1%:

n	1	2	3	4	5
	1.0000	1.0020	1.0079	1.0179	1.0321
n	6	7	8	9	10
	1.0506	1.0736	1.1015	1.1347	1.1734

We conclude from this numerical experiment that our methods are applicable in a straightforward fashion for ratios roughly above 2-3%.

Now, what does the biology tell us about the ratio σ/a ? In the cat area 17 (analog to V1 in humans), it is commonly agreed that excitatory connections can span as much as 8mm whereas inhibitory are limited to 3mm for an area which is roughly 25x20mm, hence a ratio between 12% and 32%. In humans, less data is available but Bressloff et al. in [12] use a lateral connectivity function spanning 10mm for an area V1 with area 144x96mm, hence a ratio of roughly 7%. In both species we are well in the range of separations of the eigenvalues that poses no numerical problems to the continuation methods.

7.2. How steep should the sigmoid be?. When the slope λ of the sigmoid in the model increases without bound, the sigmoid converges toward the Heaviside function. As shown in the paper, when λ increases, we predict the appearance of a variety of new stationary solutions of the neural field equations. From the biological viewpoint one observes hard thresholds at the level of single neurons f-I curves [33], the curves that relate the external current to the firing rate. At the population level, the one described by the neural field equations, these hard thresholds are smoothed over by the effect of population averaging. Our mathematical analysis can provide an answer to the question of how steep is a sigmoid from a biological perspective. The answer is related, in the case of the ring model, to the connection between the slope parameter λ and the connectivity function \mathbf{J} . As shown in equation (5.1) the relevant parameter is the product $\lambda|J_0|$ which is constrained by a) the fact that it must be larger than the first bifurcation value in order for the model to produce tuning curves, and b) that it must be smaller than the value for which the tuning curves saturate, hence do not vary with the contrast anymore, in contradiction with the biological measurements. For each application of the neural field equations this is how the biology enters the mathematics to constrain the model parameter values.

8. Conclusion. In this paper we have pursued the analysis, started in [24, 26], of a special type of integro-differential equation that appears in neural field and neural mass models where we are interested in approximating mesoscopic and macroscopic ensembles of neurons by continuous descriptions. We call these equations neural equations. Like in these two previous papers our approach is based on functional analysis to obtain clean results about the well-posedness of these equations from which we can study the questions of existence and uniqueness of the solutions. In this article we have enforced more spatial regularity by choosing the Sobolev, and Hilbert, space $\mathbf{W}^{m,2}(\Omega)$ instead of the space $\mathbf{L}^2(\Omega)$ that we used previously. The reason for this change is not only technical, it allows us to study the question of the bifurcation of the solutions, while ensuring that the membrane potential (or the activity) remains finite on the cortex.

In effect these equations depend upon a number of biological or experimental parameters such as the slope λ of the nonlinearity, the connectivity matrix \mathbf{J} , or the input \mathbf{I} . These parameters vary in general in neural populations because of such processes as plasticity and learning. It is therefore important to understand how the solutions of these equations vary when these parameters change. To this end, we used two theories: the degree theory and the bifurcation theory. The degree theory does not require the above spatial regularity because it describes the general behaviour of the cortical states as the parameters vary. On the other hand, the bifurcation theory describes the precise local behaviours of the cortical states as the parameters vary and requires spatial regularity to be able to complete the numerical computations.

We believe that a good model should exhibit bounded membrane potentials which requires to take a bounded nonlinearity (as opposed to some papers, see for example [4]). The degree theory yields the powerful estimate that the number of persistent states has to be odd, hence it predicts an additional persistent state in the neighbourhood of pitchfork/transcritical bifurcation points. This extra point is invisible to bifurcation theory, which is a local theory (This was conjectured numerically in [21]). It may change drastically the dynamics and shows that local analysis is not sufficient for the study of the neural field equations.

We have focused on the description of the stationary solutions of the neural equations when varying the slope parameter, and tried to compute numerically the additional persistent state given by the degree theory for arbitrary external current and connectivity. As the set of stationary solutions may not be connected, we used a multiparameter continuation scheme in order to compute non-connected branches of solutions and were able to show examples of these (see sections 5 and 6). Whether these different branches of solutions intersect or are unbounded is still unknown in the general case. However, the scalar case for a one-dimensional cortex ($p = 1$, $d = 1$, $\mathbf{I}_{ext} = 0$) is almost completely solved (see section.3.1.1). This point has never been mentioned in the literature to our knowledge. The question of whether we have computed all the solutions by using our multiparameter scheme is unfortunately still open.

To summarize, using a bounded nonlinearity for the firing rate introduces new stationary solutions that were not predicted before. This suggests that the analysis of neural field models (of the visual system or of the memory for example) should be re-examined. This is the focus of our current efforts.

Acknowledgements. We thank M.E. Hendersen for his valuable help in using the library Multifario (part of Trilinos). Much of this work would have proved difficult - if not impossible - without his help. We also thank D. Wassermann for his patience and constant help in programming, the two anonymous reviewers for their helpful comments.

Appendix A. Well-posedness of operators. We prove proposition 2.3.

Proof. The integral in the right-hand side of (2.2) exists because for almost all $\mathbf{r} \in \Omega$ the p^2 elements $W_{ij}(\mathbf{r}, \cdot, t)$, $i, j = 1, \dots, p$ of \mathbf{J} are in $L^2(\Omega)$ for all $t > 0$ and the p coordinates of $\mathbf{V}(\cdot, t)$ are in $L^2(\Omega)$ for all $t > 0$.

For each $t > 0$ this right-hand side defines an element of $\mathbf{W}^{m,2}(\Omega)$. Because of Fubini's theorem it is clear that $[\mathbf{J}(t) \cdot \mathbf{V}(t)]$ is an element of $\mathbf{L}^2(\Omega)$ for all $t > 0$.

Next, for each multi-index α , $|\alpha| \leq m$, $D^\alpha[\mathbf{J}(t) \cdot \mathbf{V}(t)]$ is defined by

$$\langle D^\alpha[\mathbf{J}(t) \cdot \mathbf{V}(t)], \Phi \rangle_{\mathbf{L}^2(\Omega)} = (-1)^{|\alpha|} \langle [\mathbf{J}(t) \cdot \mathbf{V}(t)], D^\alpha \Phi \rangle_{\mathbf{L}^2(\Omega)},$$

for all Φ in $\mathbf{C}_0^\infty(\Omega, \mathbb{R}^p)$, the space of infinitely differentiable \mathbb{R}^p -valued functions defined on Ω with compact support. Applying Fubini's theorem again we obtain that the right-hand side of the previous equality is equal to

$$\langle [D^\alpha \mathbf{J}(t) \cdot \mathbf{V}(t)], \Phi \rangle_{\mathbf{L}^2(\Omega)}.$$

This proves that $D^\alpha[\mathbf{J}(t) \cdot \mathbf{V}(t)]$ exists for all $t > 0$, all multi-indexes α , $|\alpha| \leq m$, and is equal to $[D^\alpha \mathbf{J}(t) \cdot \mathbf{V}(t)]$. To see that it is in $\mathbf{L}^2(\Omega)$ just apply Fubini's theorem again. \square

Appendix B. Fixed points theorems. We briefly describe some applications of Brouwer's and Leray-Schauder's degree theories. They are central in the proofs of parts 4 and 5 of proposition 2.9.

We first recall Schaeffer's theorem and provide a short proof based on the Leray-Schauder degree.

THEOREM B.1 (Schaeffer). *Let X be a real Banach space. Suppose $M : X \rightarrow X$ is a compact mapping and*

$$\mathcal{S} = \{x \in X \mid \exists t \in [0, 1] \text{ such that } x = tM(x)\}$$

is bounded. Then M has a fixed point.

Proof. We provide for completeness a short proof based on Leray-Schauder's degree theory. Taking $r > 0$ large enough such that $\mathcal{S} \subset B_r^0$, we define $m(x, t) = x - tM(x)$ on $\bar{B}_r \times [0, 1]$. Then $0 \notin m(\partial B_r \times [0, 1])$ by construction. According to the homotopy invariance of the Leray-Schauder degree

$$\deg_{\text{LS}}(\text{Id} - M, B_r, 0) = \deg_{\text{LS}}(\text{Id}, B_r, 0) = 1 \neq 0,$$

thus, according to the Kronecker property of the Leray-Schauder degree, there exists a solution to the equation $M(x) = x$. \square

We can apply this theorem to prove existence of solutions to equation (2.10). We consider the function $\tilde{F} : \mathcal{F} \rightarrow \mathcal{F}$ defined by:

$$\tilde{F}(\mathbf{V}, \lambda) = -F(\mathbf{V}, \lambda) + \mathbf{V} = \mathbf{J} \cdot \mathbf{S}(\lambda \mathbf{V}) + \mathbf{I},$$

where F is defined in equation (2.10).

It is known that \tilde{F} is a nonlinear compact operator of \mathcal{F} [26]. We can apply Schaeffer's theorem to the function \tilde{F} since it is easy to prove (see [26]) that for all \mathbf{V} such that $\tilde{F}(\mathbf{V}, \lambda) = t\mathbf{V}$ the following holds

$$\|\mathbf{V}\|_{\mathcal{F}} \leq t(\lambda \sqrt{p} |\Omega| \|\mathbf{J}\|_F + \|\mathbf{I}\|_{\mathcal{F}}), \quad (\text{B.1})$$

where $\|\cdot\|_F$ is the Frobenius norm.

Hence for all λ there exists \mathbf{V}_λ^f such that

$$\tilde{F}(\mathbf{V}_\lambda^f, \lambda) = \mathbf{V}_\lambda^f$$

The following easy consequence of the proof of theorem B.1 is used in the article.

COROLLARY B.2. *For each $\lambda \geq 0$ there exists an open bounded set \mathcal{U}_λ containing \mathcal{S} (defined in theorem B.1) such that $\deg_{\text{LS}}(\text{Id} - \tilde{F}, \mathcal{U}_\lambda, 0) = 1$.*

We next give without proof a theorem due to Leray and Schauder.

THEOREM B.3 (Leray-Schauder). *Let X be a real normed space, $J = [a, b]$ and $M : X \times J \rightarrow X$ be of the form $\text{Id} + m$ with $m : X \times J \rightarrow X$ compact on $X \times J$. Let*

$$\Sigma = \{(x, \lambda) \in X \times J : M(x, \lambda) = 0\}$$

and for each $\lambda \in J$, let

$$\Sigma_\lambda = \{x \in X : (x, \lambda) \in \Sigma\}$$

Assume that Σ_a is bounded and that

$$\deg_{\text{LS}}(M(\cdot, a), \mathcal{U}, 0) \neq 0$$

for some open bounded set $\mathcal{U} \supset \Sigma_a$.

Then Σ contains a connected component \mathcal{C} intersecting $\Sigma_a \times \{a\}$ and which either intersects $\Sigma_b \times \{b\}$ or is unbounded.

Appendix C. Compact operators with simple eigenvalues.

PROPOSITION C.1. *For every $m \in \mathbb{N}^*$, the set of compact operators with m simple first eigenvalues is dense in the set of compact operators.*

Proof. The set $\mathcal{R}_f(\mathcal{F})$ of finite dimensional range linear operators is dense in the set \mathcal{H} of the linear compact operators of \mathcal{F} [13]. Thus we only need to prove the theorem for $\mathcal{R}_f(\mathcal{F})$. Let us consider $\mathbf{J} \in \mathcal{R}_f(\mathcal{F})$, and $R(\mathbf{J}) = \text{Span}(e_1, \dots, e_k)$, $k \geq m$. Without loss of generality we assume that the first eigenvalue of \mathbf{J} has multiplicity two, i.e. $\beta_1 = \beta_2$. Its corresponding Jordan block is then

$$\begin{bmatrix} \beta_1 & \varepsilon \\ 0 & \beta_1 \end{bmatrix}$$

Then if we define $\mathbf{J}_n = \mathbf{J} + \frac{1}{n}e_2 \otimes e_2$, we have $\lim_{n \rightarrow \infty} \mathbf{J}_n = \mathbf{J}$. The first two eigenvalues β_1 and $\beta_1 + \frac{1}{n}$ of \mathbf{J}_n are simple, i.e. $\mathbf{J}_n e_1 = \beta_1 e_1$ and $\mathbf{J}_n (n\varepsilon e_1 + e_2) = (\beta_1 + \frac{1}{n})(n\varepsilon e_1 + e_2)$. We can do the same for the other eigenvalues, and define an operator \mathbf{J}_n with m simple first eigenvalues, a finite dimensional rank, and which is arbitrarily close to \mathbf{J} . \square

PROPOSITION C.2. *The same proposition holds for operators of the type $\text{Id} + \mathbf{J}$ where \mathbf{J} is a compact operator.*

Proof. It follows from that of C.1. \square

Appendix D. Reduction of the activity based model to a finite number of ordinary differential equations. We consider the equation for the activity-based model:

$$\begin{cases} \dot{\mathbf{A}} &= -\mathbf{L}_a \cdot \mathbf{A} + \mathbf{S}_\lambda (\mathbf{J} \cdot \mathbf{A} + \mathbf{I}) & t > 0 \\ \mathbf{A}(\cdot, 0) &= \mathbf{A}_0(\cdot) \end{cases} \quad (\text{D.1})$$

We recall that $\mathbf{L}_a \neq \mathbf{L}$ (see [20]) because they do not have the same biological meaning: One is related to the synaptic time constant and the other to the cell membrane time constant. We let $\mathbf{L}_a = \text{diag}(\alpha_1, \dots, \alpha_p)$

We also recall the PG-kernel decomposition of $\mathbf{J} = \sum_k X_k \otimes Y_k$

Each of the p coordinates $A_i, i = 1, \dots, p$ of \mathbf{A} satisfies

$$\dot{A}_i + \alpha_i A_i = \mathbf{S}_\lambda(\mathbf{J} \cdot \mathbf{A} + \mathbf{I})_i \quad i = 1, \dots, p$$

Similarly to the voltage case, let us consider the p finite dimensional subspaces $F_i, i = 1, \dots, p$ of \mathcal{G} , where each F_i is generated by the N elements $Y_k^i, k = 1, \dots, N$. We decompose \mathcal{G} as the direct sum of F_i and its orthogonal complement for $\langle \cdot, \cdot \rangle_2$ $F_i^\perp, \mathcal{G} = F_i \oplus F_i^\perp$ and write $A_i = A_i^\parallel + A_i^\perp$. We note \prod_i^\parallel (respectively \prod_i^\perp) the projection from \mathcal{G} to F_i (respectively to F_i^\perp) parallel to F_i^\perp (respectively to F_i). This induces a decomposition of \mathcal{F} as the direct sum of $F = \prod_{i=1}^p F_i$ and $F^\perp = \prod_{i=1}^p F_i^\perp$ such that for each vector \mathbf{A} of \mathcal{F} we can write $\mathbf{A} = \mathbf{A}^\parallel + \mathbf{A}^\perp$. By construction we also have

$$\mathbf{J} \cdot \mathbf{A}^\perp = 0,$$

and therefore

$$\begin{cases} \dot{A}_i^\parallel + \alpha_i A_i^\parallel = \prod_i^\parallel \mathbf{S}_\lambda(\mathbf{J} \cdot \mathbf{A}^\parallel + \mathbf{I})_i \\ \dot{A}_i^\perp + \alpha_i A_i^\perp = \prod_i^\perp \mathbf{S}_\lambda(\mathbf{J} \cdot \mathbf{A}^\parallel + \mathbf{I})_i \end{cases} \quad i = 1, \dots, p$$

which is a $2p$ -dimensional non-autonomous system of ODEs:

$$\begin{cases} \dot{\mathbf{A}}^\parallel + \mathbf{L}_a \cdot \mathbf{A}^\parallel = \prod^\parallel \mathbf{S}_\lambda(\mathbf{J} \cdot \mathbf{A}^\parallel + \mathbf{I}) \\ \dot{\mathbf{A}}^\perp + \mathbf{L}_a \cdot \mathbf{A}^\perp = \prod^\perp \mathbf{S}_\lambda(\mathbf{J} \cdot \mathbf{A}^\parallel + \mathbf{I}) \end{cases},$$

where $\prod^\parallel \mathbf{A} = (\prod_i^\parallel A_i)_{i=1, \dots, p}$ and $\prod^\perp \mathbf{A} = (\prod_i^\perp A_i)_{i=1, \dots, p}$ are the projections of \mathbf{A} on F and F^\perp .

The first equation is a p -dimensional autonomous system of ODEs, which can be solved before solving the second one.

D.1. Lemmas. LEMMA D.1. *For all $x, \lambda \in \mathbb{R}$ we have*

$$(S(\lambda x) - S(0))^2 \leq S(\lambda^2 x^2) - S(0)$$

Proof. We set $X = \lambda x$ and consider two cases.

$X > 1$ We have $e^{-X} > e^{-X^2}$ and therefore $S(X) - 1/2 < S(X^2) - 1/2$. Moreover, since $S(X) - 1/2 < 1, (S(X) - 1/2)^2 < S(X) - 1/2$ and we are done.

$0 < X < 1$ We let $X = \log y, 1 < y < e$. We therefore have

$$S(X) - 1/2 = \frac{1}{2} \frac{y-1}{y+1} \quad S(X^2) - 1/2 = \frac{1}{2} \frac{y^{\log y} - 1}{y^{\log y} + 1}$$

We consider the expression $(y-1)^2(y^{\log y} + 1) - 2(y+1)^2(y^{\log y} - 1)$ and prove it is negative. Because $y^{\log y} < y$ it is upperbounded by $(y-1)^2(y^{\log y} + 1) - 2(y^{\log y} + 1)^2(y^{\log y} - 1)$ which has the sign of $(y-1)^2 - 2(y^{2 \log y} - 1)$. The last expression is upperbounded by $(y-1)^2 - 2(y^{\log y} - 1) = (e^X - 1)^2 - 2(e^{X^2} - 1)$ which is negative for $0 < X < 1$.

□

PROPOSITION D.2. *The solutions of equation (2.10) satisfy the following inequalities for all $\lambda \geq 0$*

$$\left\| \mathbf{V}_\lambda^f \right\|_{\mathcal{F}} \leq \sqrt{p|\Omega|} \|\mathbf{J}\|_{\mathcal{F}} + \|\mathbf{I}_{\text{ext}}\|_{\mathcal{F}} \stackrel{\text{def}}{=} B_1$$

$$\left\| \mathbf{V}_\lambda^f - \mathbf{V}_0^f \right\|_{\mathcal{F}} \leq \frac{1}{2} \sqrt{p|\Omega|} \|\mathbf{J}\|_{\mathcal{F}} \stackrel{\text{def}}{=} B_2,$$

as well as

$$\left\| \mathbf{V}_\lambda^f - \mathbf{V}_0^f \right\|_{\mathcal{F}} \leq \frac{\lambda}{4} \|\mathbf{J}\|_{\mathcal{F}} B_1$$

Proof. The first inequality is a straightforward consequence of equation (2.10), taking the \mathcal{F} -norm and using the fact that $0 \leq S(x) \leq 1$ for all $x \in \mathbb{R}$.
For the second one we write $\mathbf{V}_\lambda^f - \mathbf{V}_0^f = \mathbf{J} \cdot (\mathbf{S}(\lambda \mathbf{V}_\lambda^f) - \mathbf{S}(0))$, take the \mathcal{F} -norm of both sides of the equality and use the Cauchy-Schwarz inequality. We find $\left\| \mathbf{V}_\lambda^f - \mathbf{V}_0^f \right\|_{\mathcal{F}} \leq \|\mathbf{J}\|_{\mathcal{F}} \cdot \left\| \mathbf{S}(\lambda \mathbf{V}_\lambda^f) - \mathbf{S}(0) \right\|_{\mathbf{L}^2(\Omega, \mathbb{R}^p)}$. But since $\forall x \in \mathbb{R}$, $-\frac{1}{2} \leq S(x) - S(0) \leq \frac{1}{2}$, we have $\left\| \mathbf{S}(\mathbf{V}_\lambda^f) - \mathbf{S}(0) \right\|_{\mathbf{L}^2(\Omega, \mathbb{R}^p)} \leq \frac{1}{2} \sqrt{p|\Omega|}$, which proves the first inequality.

The third inequality can be obtained as follows. It is easy to see that $S(\lambda x) - S(0) \leq \frac{\lambda}{4}|x|$ for all $x \in \mathbb{R}$ and all $\lambda \geq 0$. This implies that $\left\| \mathbf{S}(\mathbf{V}_\lambda^f) - \mathbf{S}(0) \right\| \leq \frac{\lambda}{4} \left\| \mathbf{V}_\lambda^f \right\|$. The first inequality yields the third. \square

Appendix E. An equality for the adjoint operator. We prove proposition 3.2.

Proof. We prove the proposition in the case $m = p = 1$. By definition of $\mathbf{J}_{\mathcal{F}}^*$ we have

$$\langle \mathbf{U}, \mathbf{J}_{\mathcal{F}}^* \cdot \mathbf{V} \rangle_{\mathcal{F}} = \langle \mathbf{J} \cdot \mathbf{U}, \mathbf{V} \rangle_{\mathcal{F}} \quad \forall \mathbf{U}, \mathbf{V} \in \mathcal{F}$$

We note $\mathbf{X} = \mathbf{J}_{\mathcal{F}}^* \cdot \mathbf{V}$ and rewrite the previous equation as

$$\langle \mathbf{U}, \mathbf{X} \rangle_2 + \langle \nabla \mathbf{U}, \nabla \mathbf{X} \rangle_2 = \langle \mathbf{J} \cdot \mathbf{U}, \mathbf{V} \rangle_{\mathcal{F}}$$

We next rewrite the right-hand side

$$\langle \mathbf{J} \cdot \mathbf{U}, \mathbf{V} \rangle_{\mathcal{F}} = \langle \mathbf{J} \cdot \mathbf{U}, \mathbf{V} \rangle_2 + \langle \nabla (\mathbf{J} \cdot \mathbf{U}), \nabla \mathbf{V} \rangle_2$$

The crucial step is to observe that

$$\langle \nabla (\mathbf{J} \cdot \mathbf{U}), \nabla \mathbf{V} \rangle_2 = \langle \mathbf{U}, (\nabla_1 \mathbf{J})_2^* \cdot \nabla \mathbf{V} \rangle_2,$$

where ∇_1 indicates the derivative with respect to the first variable, i.e.

$$(\nabla_1 \mathbf{J})_2^* \cdot \nabla \mathbf{V}(\mathbf{r}) = \sum_{i=1}^d \int_{\Omega} \frac{\partial \mathbf{J}}{\partial r'_i}(\mathbf{r}', \mathbf{r}) \frac{\partial \mathbf{V}}{\partial r'_i}(\mathbf{r}') d\mathbf{r}'$$

Let us fix \mathbf{V} in \mathcal{F} . \mathbf{X} is the solution of

$$\langle \mathbf{U}, \mathbf{X} \rangle_2 + \langle \nabla \mathbf{U}, \nabla \mathbf{X} \rangle_2 = \langle \mathbf{U}, f \rangle_2 \quad \forall \mathbf{U} \in \mathcal{F}$$

Hence \mathbf{X} is the unique weak solution in \mathcal{F} of the homogeneous Neumann problem

$$\begin{cases} -\Delta \mathbf{X} + \mathbf{X} &= f & \text{on } \Omega \\ \frac{\partial \mathbf{X}}{\partial \nu} &= 0 & \text{on } \partial \Omega \end{cases}$$

f is the element of $\mathbf{L}^2(\Omega)$ defined by

$$f = \mathbf{J}_2^* \cdot \mathbf{V} + (\nabla_1 \mathbf{J})_2^* \cdot \nabla \mathbf{V} +$$

The regularity properties of the solutions of elliptic equations [23, Chapter 6] imply that \mathbf{X} is in $\mathbf{W}^{2,2}(\Omega)$. Let us denote by \mathcal{D} the differential operator, defined in $\mathbf{W}^{2,2}(\Omega)$ by

$$\mathcal{D} = -\Delta + \text{Id}$$

We now choose $\mathbf{V} = e_{\mathcal{F}}^*$. This implies that $\mathbf{X} = \lambda e_{\mathcal{F}}^*$ and hence $\frac{\partial e_{\mathcal{F}}^*}{\partial \nu} = 0$ in $\partial\Omega$. Furthermore we have

$$\lambda \mathcal{D} \cdot e_{\mathcal{F}}^* = \mathbf{J}_2^* \cdot e_{\mathcal{F}}^* + (\nabla_1 \mathbf{J})_2^* \cdot \nabla e_{\mathcal{F}}^*$$

Green's formula with the condition $\frac{\partial e_{\mathcal{F}}^*}{\partial \nu} = 0$ show that

$$(\nabla_1 \mathbf{J})_2^* \cdot \nabla e_{\mathcal{F}}^* = -\mathbf{J}_2^* \cdot \Delta e_{\mathcal{F}}^*,$$

and therefore we have

$$\lambda \mathcal{D} \cdot e_{\mathcal{F}}^* = \mathbf{J}_2^* \cdot (\mathcal{D} \cdot e_{\mathcal{F}}^*),$$

which shows that $\mathcal{D} \cdot e_{\mathcal{F}}^*$ is an eigenvector of \mathbf{J}_2^* associated with the eigenvalue λ . We can choose $e_{L^2}^*$ and $e_{\mathcal{F}}^*$ so that

$$\mathcal{D} \cdot e_{\mathcal{F}}^* = e_{L^2}^*.$$

From Green's formula

$$\langle \mathbf{U}, e_{\mathcal{F}}^* \rangle_{\mathcal{F}} = \langle \mathbf{U}, \mathcal{D} \cdot e_{\mathcal{F}}^* \rangle_2 - \int_{\partial\Omega} \frac{\partial e_{\mathcal{F}}^*}{\partial \nu} \mathbf{U} \, d\sigma,$$

and the conclusion follows from the fact that $\mathcal{D} \cdot e_{\mathcal{F}}^* = e_{L^2}^*$ and $\frac{\partial e_{\mathcal{F}}^*}{\partial \nu} = 0$ on $\partial\Omega$. \square

Appendix F. The size of the basin of attraction of a stable persistent state. In order to get a rough estimate of the size of the basin of attraction of a stable stationary solution of the neural field equations we prove the following, general, lemma.

LEMMA F.1. *Let x^f be a stable stationary solution of the finite dimensional dynamical system $\dot{x} = f(x)$ at which the Jacobian matrix A is symmetric. If the second order derivative $D^2 f$ is bounded ($\|D^2 f\|_{\infty} < \infty$), the stable manifold of x^f contains the open ball $B(x^f, R)$ with $R = 2 \frac{\min |\sigma(A)|}{\|D^2 f\|_{\infty}}$, where $\sigma(A)$ is the spectrum of the Jacobian matrix A .*

Proof. We assume w.l.g. that $x^f = 0$. We write $A = Df(0)$ and $f(x) = Ax + \epsilon(x)$, then it is known, and easy to verify, that $L(x) = \int_0^{\infty} \|e^{sA} x\|^2 ds$ is a Lyapunov function. Moreover, because of the Taylor's formula without remainder we have

$$\epsilon(x) = \left(\int_0^1 (1-s) D^2 f(sx) \, ds \right) \cdot (x, x),$$

from which we deduce that

$$\|\epsilon(x)\| \leq \frac{1}{2} \|x\|^2 \|D^2 f\|_{\infty}.$$

Let us compute

$$DL(x) \cdot f(x) = DL(x) \cdot (Ax + \epsilon(x)) = -\|x\|^2 + DL(x) \cdot \epsilon(x)$$

Now $DL(x) \cdot h = -\langle A^{-1}x, h \rangle$ and since A is symmetric, we obtain $|DL(x) \cdot h| \leq \frac{1}{\min |\sigma(A)|} \|x\| \|h\|$ and finally

$$DL(x) \cdot f(x) \leq \|x\|^2 \left(-1 + \frac{1}{2} \|D^2 f\|_{\infty} \frac{1}{\min |\sigma(A)|} \|x\| \right) < 0$$

if $\|x\| < 2 \frac{\min |\sigma(A)|}{\|D^2 f\|_{\infty}} \equiv R$ \square

REFERENCES

- [1] R. ADAMS, *Sobolev spaces*, vol. 65 of Pure and Applied Mathematics, Series of Monographs and Textbooks, Academic Press, Inc., New York, San Francisco, London, 1975.
- [2] S.-I. AMARI, *Dynamics of pattern formation in lateral-inhibition type neural fields*, Biological Cybernetics, 27 (1977), pp. 77–87.
- [3] FATIHCAN M. ATAY AND AXEL HUTT, *Stability and bifurcations in neural fields with finite propagation speed and general connectivity*, SIAM Journal on Applied Mathematics, 65 (2005), pp. 644–666.
- [4] R. BEN-YISHAI, RL BAR-OR, AND H. SOMPOLINSKY, *Theory of orientation tuning in visual cortex*, Proceedings of the National Academy of Sciences, 92 (1995), pp. 3844–3848.
- [5] P. BLOMQUIST, J. WYLLER, AND G.T. EINEVOLL, *Localized activity patterns in two-population neuronal networks*, Physica D, 206 (2005), pp. 180–212.
- [6] P.C. BRESSLOFF, *Traveling fronts and wave propagation failure in an inhomogeneous neural network*, Physica D: Nonlinear Phenomena, 155 (2001), pp. 83–100.
- [7] ———, *Spatially periodic modulation of cortical patterns by long-range horizontal connections*, Physica D: Nonlinear Phenomena, 185 (2003), pp. 131–157.
- [8] P. BRESSLOFF, *Spontaneous symmetry breaking in self-organizing neural fields*, Biological Cybernetics, 93 (2005), pp. 256–274.
- [9] P.C. BRESSLOFF, *Weakly interacting pulses in synaptically coupled neural media*, SIAM Journal on Applied Mathematics, 66 (2006), pp. 57–81.
- [10] P.C. BRESSLOFF, N.W. BRESSLOFF, AND J.D. COWAN, *Dynamical mechanism for sharp orientation tuning in an integrate-and-fire model of a cortical hypercolumn*, Neural computation, 12 (2000), pp. 2473–2511.
- [11] P.C. BRESSLOFF AND J.D. COWAN, *An amplitude equation approach to contextual effects in visual cortex*, Neural computation, 14 (2002), pp. 493–525.
- [12] P.C. BRESSLOFF, J.D. COWAN, M. GOLUBITSKY, P.J. THOMAS, AND M.C. WIENER, *Geometric visual hallucinations, euclidean symmetry and the functional architecture of striate cortex*, Phil. Trans. R. Soc. Lond. B, 306 (2001), pp. 299–330.
- [13] H. BREZIS, *Analyse fonctionnelle. Théorie et applications*, Masson, 1983.
- [14] G. CHOQUET, *Cours d'Analyse*, vol. II, Masson, 1969.
- [15] C.L. COLBY, J.R. DUHAMEL, AND M.E. GOLDBERG, *Oculocentric spatial representation in parietal cortex*, Cereb. Cortex, 5 (1995), pp. 470–481.
- [16] STEPHEN COOMBES, *Waves, bumps, and patterns in neural fields theories*, Biological Cybernetics, 93 (2005), pp. 91–108.
- [17] S. COOMBES AND M. R. OWEN, *Evans functions for integral neural field equations with heaviside firing rate function*, SIAM Journal on Applied Dynamical Systems, 3 (2004), pp. 574–600.
- [18] ———, *Bumps, breathers, and waves in a neural network with spike frequency adaptation*, Phys. Rev. Lett., 94 (2005).
- [19] P. DAYAN AND L.F. ABBOTT, *Theoretical Neuroscience : Computational and Mathematical Modeling of Neural Systems*, MIT Press, 2001.
- [20] BARD ERMENTROUT, *Neural networks as spatio-temporal pattern-forming systems*, Reports on Progress in Physics, 61 (1998), pp. 353–430.
- [21] G.B. ERMENTROUT AND J.D. COWAN, *Large scale spatially organized activity in neural nets*, SIAM Journal on Applied Mathematics, (1980), pp. 1–21.
- [22] GB ERMENTROUT AND JB MCLEOD, *Existence and uniqueness of travelling waves for a neural network*, in Royal Society(Edinburgh), Proceedings, vol. 123, 1993, pp. 461–478.
- [23] L.C. EVANS, *Partial Differential Equations*, vol. 19 of Graduate Studies in Mathematics, Proceedings of the American Mathematical Society, 1998.
- [24] O. FAUGERAS, F. GRIMBERT, AND J.-J. SLOTINE, *Abolute stability and complete synchronization in a class of neural fields models*, SIAM Journal of Applied Mathematics, 61 (2008), pp. 205–250.
- [25] O. FAUGERAS, J. TOUBOUL, AND B. CESSAC, *A constructive mean field analysis of multi population neural networks with random synaptic weights and stochastic inputs*, Frontiers in Computational Neuroscience, 3 (2009).
- [26] O. FAUGERAS, R. VELTZ, AND F. GRIMBERT, *Persistent neural states: stationary localized activity patterns in nonlinear continuous n-population, q-dimensional neural networks*, Neural Computation, 21 (2009), pp. 147–187.
- [27] S. FUNAHASHI, C.J. BRUCE, AND P.S. GOLDMAN-RAKIC, *Mnemonic coding of visual space in the monkey's dorsolateral prefrontal cortex*, J. Neurophysiol., 61 (1989), pp. 331–349.
- [28] J. GUCKENHEIMER AND P. J. HOLMES, *Nonlinear Oscillations, Dynamical Systems and Bifurcations of Vector Fields*, vol. 42 of Applied mathematical sciences, Springer, 1983.
- [29] D. HANSEL AND H. SOMPOLINSKY, *Modeling feature selectivity in local cortical circuits*, Methods of neuronal modeling, (1997), pp. 499–567.
- [30] M. HARAGUS AND G. IOOSS, *Local bifurcations, center manifolds, and normal forms in infinite dimensional*

- systems*, EDP Sci. Springer Verlag UTX series, 2009. To appear.
- [31] D. HENRY, *Geometric Theory of Semilinear Parabolic Equations*, vol. 840 of LNM, Springer-Verlag, 1981.
 - [32] H. KIELHÖFER, *Bifurcation Theory: An Introduction with Applications to PDEs*, Springer, 2003.
 - [33] E.M. IZHIKEVICH, *Neural excitability, spiking, and bursting*, International Journal of Bifurcation and Chaos, 10 (2000), pp. 1171–1266.
 - [34] VK JIRSA AND JAS KELSO, *Spatiotemporal pattern formation in neural systems with heterogeneous connection topologies*, Physical Review E, 62 (2000), pp. 8462–8465.
 - [35] T. KATO, *Perturbation Theory for Linear Operators*, Springer, 1995.
 - [36] Z.P. KILPATRICK, S.E. FOLIAS, AND P.C. BRESSLOFF, *Traveling pulses and wave propagation failure in inhomogeneous neural media*, SIAM Journal on Applied Dynamical Systems, 7 (2008), pp. 161–185.
 - [37] K. KISHIMOTO AND S. AMARI, *Existence and stability of local excitations in homogeneous neural fields*, Journal of Mathematical Biology, 7 (1979), pp. 303–318.
 - [38] YURI A. KUZNETSOV, *Elements of Applied Bifurcation Theory*, Applied Mathematical Sciences, Springer, 2nd ed., 1998.
 - [39] C.L. LAING, W.C. TROY, B. GUTKIN, AND G.B. ERMENTROUT, *Multiple bumps in a neuronal model of working memory*, SIAM J. Appl. Math., 63 (2002), pp. 62–97.
 - [40] CARLO R. LAING AND WILLIAM C. TROY, *PDE methods for nonlocal models*, SIAM Journal on Applied Dynamical Systems, 2 (2003), pp. 487–516.
 - [41] TIAN MA AND SHOUHONG WANG, *Bifurcation theory and applications*, vol. 53 of Nonlinear Science, World Scientific, 2005.
 - [42] E.K. MILLER, C.A. ERICKSON, AND R. DESIMONE, *Neural mechanisms of visual working memory in prefrontal cortex of the Macaque*, J. Neurosci., 16 (1996), pp. 5154–5167.
 - [43] YASUMASA NISHIURA AND MASAYASU MIMURA, *Layer oscillations in reaction-diffusion systems*, SIAM Journal on Applied Mathematics, 49 (1989), pp. 481–514.
 - [44] D.J. PINTO AND G.B. ERMENTROUT, *Spatially structured activity in synaptically coupled neuronal networks: 1. traveling fronts and pulses.*, SIAM J. of Appl. Math., 62 (2001), pp. 206–225.
 - [45] M.R. QUBBAJ AND V.K. JIRSA, *Neural field dynamics with heterogeneous connection topology*, Physical review letters, 98 (2007), p. 238102.
 - [46] P.H. RABINOWITZ, *Some global results for nonlinear eigenvalue problems*, J. Funct. Anal, 7 (1971), pp. 487–513.
 - [47] J.E. RUBIN AND W.C. TROY, *Sustained spatial patterns of activity in neuronal populations without recurrent excitation*, SIAM journal on applied mathematics, 64 (2004), pp. 1609–1635.
 - [48] MARZIO SALA, MICHAEL A. HEROUX, AND DAVID M. DAY, *Trilinos tutorial*, Tech. Report SAND2004-2189, Sandia National Laboratories, 2004.
 - [49] O. SHRIKI, D. HANSEL, AND H. SOMPOLINSKY, *Rate models for conductance-based cortical neuronal networks*, Neural Computation, 15 (2003), pp. 1809–1841.
 - [50] F.G. TRICOMI, *Integral Equations*, Dover, 1985. Reprint.
 - [51] N.A. VENKOV, S. COOMBES, AND P.C. MATTHEWS, *Dynamic instabilities in scalar neural field equations with space-dependent delays*, Physica D: Nonlinear Phenomena, 232 (2007), pp. 1–15.
 - [52] H.R. WILSON AND J.D. COWAN, *A mathematical theory of the functional dynamics of cortical and thalamic nervous tissue*, Biological Cybernetics, 13 (1973), pp. 55–80.
 - [53] K. YOSIDA, *Functional analysis. reprint of the sixth (1980) edition. classics in mathematics*, 1995.